NACA

RESEARCH MEMORANDUM

PRELIMINARY FULL-SCALE INVESTIGATION OF A $\frac{1}{3}$-SCALE

MODEL OF A CONVERTIBLE-TYPE AIRPLANE

By

Roy H. Lange, Bennie W. Cocke, Jr., and
Anthony J. Proterra

Langley Aeronautical Laboratory
Langley Air Force Base, Va.

NATIONAL ADVISORY COMMITTEE
FOR AERONAUTICS
WASHINGTON

June 7, 1949

ERRATUM

NACA RM L9C29

PRELIMINARY FULL-SCALE INVESTIGATION OF A $\frac{1}{3}$ - SCALE
MODEL OF A CONVERTIBLE-TYPE AIRPLANE
By Roy H. Lange, Bennie W. Cocke, Jr.,
and Anthony J. Proterra

June 7, 1949

Page 4, line 7: The definition of β should read as follows:

propeller-blade angle at 0.7 radius, degrees

ERRATA

NACA RM L9C29

PRELIMINARY FULL-SCALE INVESTIGATION OF A $\frac{1}{3}$-SCALE

MODEL OF A CONVERTIBLE-TYPE AIRPLANE

By Roy H. Lange, Bennie W. Cocke, Jr., and
Anthony J. Proterra

June 7, 1949

Errors in the plot of C_{T_e}/C_Q against β in figure 41 necessitate the
following changes:

Page 11, lines 16 to 19: Delete the last two sentences of this para-
graph and replace them with the following sentence:

These results show that the optimum blade angle for static thrust
(where C_{T_e}/C_Q is maximum) is less than 10°.

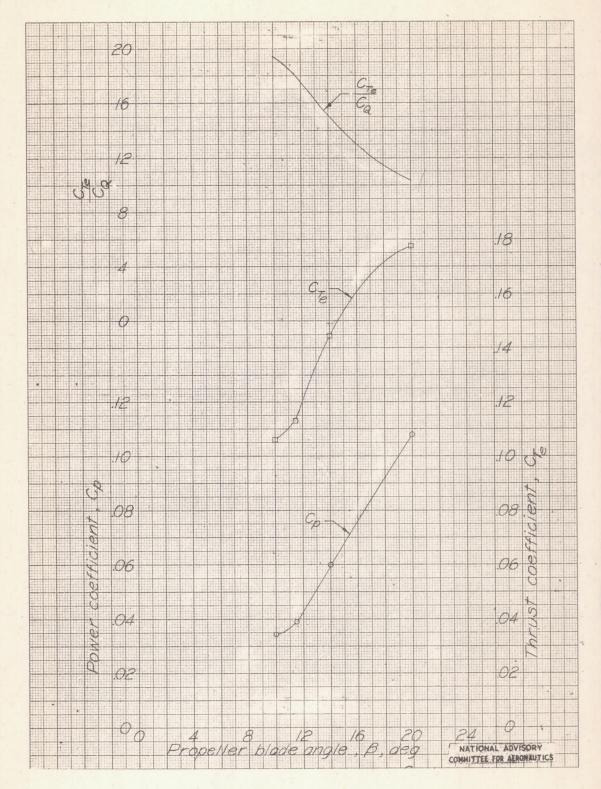Figure 41: Replace this figure with revised figure 41 attached.

Figure 41.- Variation of C_p, C_{T_e}, and C_{T_e}/C_Q with β of the model propellers. Basic model configuration; v/nD, 0; data for $\beta = 20°$ obtained with wing-tip support.

NATIONAL ADVISORY COMMITTEE FOR AERONAUTICS

———————

RESEARCH MEMORANDUM

———————

PRELIMINARY FULL-SCALE INVESTIGATION OF A $\frac{1}{3}$-SCALE

MODEL OF A CONVERTIBLE-TYPE AIRPLANE

By Roy H. Lange, Bennie W. Cocke, Jr., and
Anthony J. Proterra

SUMMARY

The results of a preliminary investigation of a $\frac{1}{3}$-scale model of a convertible-type airplane in the Langley full-scale tunnel are presented in this paper. The maximum-lift and stalling characteristics of several model configurations, the longitudinal stability characteristics of the model, and the effectiveness of the control surfaces were determined with the propellers removed. The propulsive characteristics, the effect of propeller operation on the lift, and the static thrust of the model propellers were determined at several propeller-blade angles.

The results with the propellers removed showed that the maximum lift coefficient of the complete model configuration was only 0.97 as compared with the value of 1.31 for the model configuration in which the engine air ducts and canopy are removed. The model with the propellers removed (normal center-of-gravity position) has a positive static margin, stick fixed, varying from 5 to 13 percent of the mean aerodynamic chord throughout the unstalled range of lift coefficients. The unit horizontal tail is sufficiently powerful to trim the airplane with the propellers removed throughout the unstalled range of lift coefficients.

The peak propulsive efficiencies for $\beta = 20^{\circ}$ and $\beta = 30^{\circ}$ were increased 7 percent at $C_L \cong 0.67$ and 20 percent at $C_L \cong 0.74$, respectively, with the propellers rotating upward in the center than with the propellers rotating downward in the center. Indications are that the minimum forward-flight speed of the airplane for full-power operation at sea level will be about 90 miles per hour. Decreasing the weight and increasing the power reduced this value of minimum speed and there were no indications from the results of a lower limit to the minimum speed.

INTRODUCTION

A preliminary investigation has been conducted on a $\frac{1}{3}$-scale model of a convertible-type airplane in the Langley full-scale tunnel. This airplane is of unconventional design with an almost circular plan form.

Very large diameter articulated propellers are located at the wing tips.
A unit horizontal tail is used to obtain both longitudinal and lateral
control.

The airplane is expected to assume attitudes approaching hovering
and vertical descent as a result of the relatively large static thrust
and large power effects on lift. The investigation in the Langley full-
scale tunnel was, therefore, chiefly for the purpose of determining the
longitudinal stability and the performance of the airplane in the very
high angle-of-attack range.

It was planned to make tests with the propellers removed and with
the propellers operating so that the effects of propeller operation
might be determined. The tests of the model with the propellers removed
included measurements to determine the longitudinal stability, the maximum-
lift and stalling characteristics of several model configurations, and
the effectiveness of the ailavators and the rudders. Only a small part
of the propellers-operating test program was completed when testing was
terminated by the failure and complete destruction of one of the model
propellers. The tests with the propellers operating were made at several
propeller blade angles and included measurements to determine the pro-
pulsive characteristics, the effect of propeller operation on the maximum
lift, and the static thrust of the model propellers. The data obtained
with the propellers operating were limited and were insufficient to
determine completely the stability and performance of the airplane.

COEFFICIENTS AND SYMBOLS

The results of the tests are presented as standard NACA coefficients
of forces and moments. Rolling-, yawing-, and pitching-moment coeffi-
cients are given about a center-of-gravity position located at a point
on the root chord projected into the plane of symmetry from 26.3 percent
of the mean aerodynamic chord. The positive directions of forces, of
moments, of angular displacements of the model and control surfaces, and
of hinge moments are given in figure 1.

C_L lift coefficient (L/qS)

C_D drag coefficient (D/qS)

C_m pitching-moment coefficient (M/qSc)

C_l rolling-moment coefficient (l/qSb)

C_n yawing-moment coefficient (N/qSb)

C_Y lateral-force coefficient (Y/qS)

C_h hinge-moment coefficient $(H/qb'\bar{c}^2)$

C_P　　　　　power coefficient $\left(P/\rho n^3 D^5\right)$

C_{T_e}　　　　effective thrust coefficient $\left(T_e/\rho n^2 D^4\right)$

C_Q　　　　torque coefficient $\left(Q/\rho n^2 D^5\right)$

Q_c　　　　torque coefficient $\left(Q/2qD^3\right)$

C_{D_R}　　　resultant drag coefficient $\left(D_R/qS\right)$

V/nD　　　propeller advance-diameter ratio

L　　　　lift

Y　　　　lateral force along axis

D　　　　drag of model with propellers removed or propeller diameter (5.33 ft on model)

$\left.\begin{array}{l} M \\ l \\ N \end{array}\right\}$　moments about wind axes

H　　　　hinge moment of control surface

P　　　　power input per propeller $(2\pi nQ)$

Q　　　　torque per propeller

T_e　　　effective thrust per propeller $\left(\dfrac{D_u - D_{R_u}}{2}\right)$

D_R　　　resultant drag with propellers operating

q　　　　free-stream dynamic pressure $\left(\frac{1}{2}\rho V^2\right)$

S　　　　wing area (47.444 sq ft on model)

c　　　　wing mean chord (S/b)

$\bar{c}$　　　root-mean-square chord of a control surface back of hinge line

b　　　　wing span (7.777 ft on model)

b'　　　control-surface span along hinge line

V　　　　airspeed

n　　　　propeller rotational speed

α angle of attack of thrust axis relative to free-stream direction, degrees

ρ mass density of air

δ control-surface deflection, degrees

$\delta_{a_{T_R}}$ right ailavator tab deflection, degrees

$\delta_{a_{T_L}}$ left ailavator tab deflection, degrees

β propeller-blade angle at 0.75 radius, degrees

M.A.C.   mean aerodynamic chord (6.61 ft on model)

η propulsive efficiency $\left(\dfrac{C_{T_e}}{C_P} \dfrac{V}{nD} \right)$

Subscripts:

a   ailavator (aileron or elevator)

r   rudder

f   flap

T   tab

u   uncorrected

t   tail

MODEL AND EQUIPMENT

The general arrangement and geometric characteristics of the model are given in figure 2. Control-surface data are given in table I.

The model is powered by a 200-horsepower, water-cooled, electric induction motor. Power is transmitted from the motor to the propellers by means of extension shafts through right-angle gear boxes at the wing tips. The propeller installation at each wing tip consists of 2 two-blade propellers mounted in tandem so as to form a four-blade configuration. These tandem propellers rotate in the same direction with the propellers at each wing tip rotating upward at the wing center section.

The propeller blades are free to flap fore or aft 10° from the perpendicular to the propeller axis as they rotate. The blades of each propeller are so interconnected that as one blade flaps forward the

opposite blade flaps aft. In addition, as a blade flaps forward, the hub mechanism causes the pitch to decrease and as the blade flaps aft, the pitch is increased. This load-relieving mechanism was found to be necessary by the airplane designer in his analyses from considerations of propeller stability, blade loads, and uniformity of disk-thrust loading.

The propeller torque was determined from calibration curves of motor torque as a function of minimum input current to the motor. The propeller-rotational speed was measured by a condenser-type tachometer.

The movable control surfaces on the model were hydraulically actuated by remote control. Electrical position indicators and strain gages measured control-surface deflections and hinge moments, respectively.

Two model-support arrangements were used in the tests. The original cantilever strut support was attached to the model at the left wing tip. (See fig. 3.) A revised support was attached to the model on the under side of the wing at the wing semispan during the tests to avoid the large interference effects that were found to be caused by the original wing-tip support. Both supports were located 21.6 percent of the mean aerodynamic chord aft of the leading edge of the wing root chord. The results given throughout this paper are for the model with the semispan support unless otherwise specified. The model was mounted vertically in the tunnel in order to obtain an unlimited range of angle of attack and to minimize jet-boundary effects. The value of the correction factor used in the jet-boundary-correction equations as determined from figure 4 of reference 1 was -0.13.

The Langley full-scale tunnel and balance system are described in reference 2.

METHODS AND TESTS

Force tests were made of the model for a range of angles of attack from -19° to 90°. Except where noted, the tests were made at a tunnel airspeed of approximately 87 miles per hour, corresponding to a Reynolds number of approximately 5,380,000 based on the mean aerodynamic chord of 6.61 feet. These tests were made for both the basic model and the complete model configurations (figs. 4 and 3, respectively). As shown, the basic model differs from the complete model in that the canopy and engine air ducts are removed.

Force tests and tuft observations were initially made of the model in the basic and complete configurations with the propellers removed and all control surfaces neutral. Tests of the complete model configuration with propellers removed revealed premature separation at the wing center section, resulting in low values of $C_{L_{max}}$. In an attempt to increase the $C_{L_{max}}$ of the model, the several modifications listed in

table II and shown in figures 5 to 10 were made. Tests of these modifications included lift measurements and tuft observations for a range of angles of attack in the region of the stall only.

Control effectiveness and hinge moments were determined for the ailavators acting as elevators and ailerons, for the stability flaps, and for the rudders for the model with the propellers removed and at zero yaw. The effectiveness of the ailavator tab was also determined. Hinge moments of the control surfaces were determined on the right side of the model only.

Elevator-effectiveness tests were made in the region of longitudinal trim for a wide range of angles of attack. For angles of attack greater than 24° the elevators were deflected only over a small range near maximum negative deflection. The aileron effectiveness was determined by first deflecting both left and right ailavators to the approximate position for longitudinal trim at each angle of attack. With the left ailavator fixed at the setting for longitudinal trim, the right ailavator was deflected $\pm 15^\circ$ from this trim position. The effectiveness of the stability flap and the rudder was determined over a large range of flap and rudder deflections with the ailavators set at the approximate deflection for longitudinal trim at each angle of attack.

Force tests were made with the model in the basic configuration with the propellers operating at $\beta = 20^\circ$ and $\beta = 30^\circ$ to determine the propulsive characteristics for a large angle-of-attack range. In order to obtain data over the complete V/nD range of the propellers, tests were made as follows for each angle of attack: first, with the propellers set at the maximum rpm as limited by the available torque, the tunnel airspeed was varied in steps from zero to approximately 87 miles per hour; second, with the tunnel airspeed held constant at approximately 87 miles per hour, the propeller speed was increased from the windmilling to the maximum speed in increments of 100 rpm.

The aerodynamic characteristics of the model with the propellers operating at blade angles of 10°, 11.5°, and 14° were determined from force tests at angles of attack ranging from 3° to 84°. The purpose of these tests was to choose optimum propeller-blade angles for simulating the propeller-operating conditions of the airplane in the very high angle-of-attack range. For these tests the propellers were operated through a V/nD range sufficient only to obtain an intersection of the model Q_c against C_L curve at constant angle of attack with the airplane Q_c against C_L curve for full-power operation. (See fig. 11.)

The static thrust of the model propellers was determined from tests at blade angles of 10°, 11.5°, and 14° at an angle of attack of 90°, and from tests at a blade angle of 20° at an angle of attack of 74° with the model supported at the wing tip. At each blade angle, measurements were made for the conditions of maximum propeller rpm as limited by the available torque and zero tunnel airspeed.

RESULTS AND DISCUSSION

The data have been corrected for balance alinement, blocking, and jet-boundary effects. Tare corrections were applied to the propellers-removed drag data only.

The presentation of the test results and the analysis of the data have been grouped into two main sections. The first section gives the results of the propellers-removed investigations to determine the maximum-lift and stalling characteristics of the model, the longitudinal stability characteristics of the model, and the effectiveness of the control surfaces. The second section gives the results of propeller-operating investigations of the propulsive characteristics of the model-propellers combination, the static thrust of the model propellers, and the maximum lifts obtainable for simulated flight conditions.

Results with Propellers Removed

<u>Maximum-lift and stalling characteristics</u>.- The results of the maximum-lift and stall tests are presented in figures 12 to 14 and the test data are summarized in table II. Photographs of wool tufts, placed at frequent intervals on the upper wing surface, to show the disposition of the air flow over the model at several angles of attack are shown in figure 15 for the basic-model and complete-model configurations.

With the model in the complete configuration (fig. 12) the maximum lift coefficient obtained was 0.97 at an angle of attack of $32°$. Tuft observations indicated that premature stall probably occurred from disturbances just aft of the canopy and in the region of the engine air ducts. (See fig. 15(a).) As a result, several modifications to the canopy and the engine air ducts were tested in an attempt to delay premature stalling at these locations. Opening the canopy, installing fillets around the engine air ducts, and unsealing the engine-air outlets did not change the value of $C_{L_{max}}$. (See table II.) Increases in $C_{L_{max}}$ of 0.06 and 0.08, respectively, were obtained by extending the canopy afterbody as shown in figure 6 and by installing extended spinners in the engine air ducts as shown in figure 8. Details of the extended-spinner installation are shown in figure 9. Removing the engine air ducts and fairings increased the $C_{L_{max}}$ of the model by 0.22 over that for the complete model configuration. It should be pointed out that the cooling fans to be used on the airplane in the engine air ducts were not duplicated on the model. Tests with only the canopy removed increased the $C_{L_{max}}$ by 0.07. A maximum lift coefficient of 1.31 was obtained for the model in the basic model configuration. (See fig. 14.) Tuft studies indicated that the air flow over the model in the basic configuration was smooth and that no appreciable disturbances occurred even in the region of the propeller nacelle-wing juncture up to the angle of stall. (See fig. 15(b).)

Static-longitudinal-stability tests.- The variations of C_m, C_{h_a}, C_L, and C_D with ailavator deflection δ_a for the complete model configuration are shown in figures 16 to 19. From these figures, curves were obtained to show the variations of $(\partial C_m/\partial \delta_a)_{C_m=0}$ and $(\partial C_{h_a}/\partial \delta_a)_{C_{h_a}=0}$ with C_L and are given in figure 20. The ailavator effectiveness $\partial C_m/\partial \delta_a$ is approximately constant and equal to -0.0052 throughout the lift-coefficient range from 0 to 0.8. The slope $\partial C_{h_a}/\partial \delta_a$ varies from approximately 0 to -0.011 for a C_L range from 0 to 0.5. There is a reversal of slope in the range between $C_L = 0.5$ and $C_L = 0.8$.

As an indication of the static longitudinal stability of the complete model configuration with the propellers removed, curves showing the variations of C_m with C_L for constant ailavator settings are given in figure 21. The values of $\partial C_m/\partial C_L$ near the trim indicate that the airplane will be longitudinally stable for the lift-coefficient range from 0 to 0.63.

In order to show more clearly the static longitudinal stability characteristics of the airplane, the fore and aft locations of the stick-fixed neutral point have been computed by method 1 of reference 3 and are presented in figure 22. These results show that for the normal center-of-gravity location the airplane with propellers removed will have a positive static margin varying from 5 to 13 percent of the mean aerodynamic chord throughout the unstalled range of lift coefficients.

The magnitude of the ailavator deflections required to trim the airplane for lift coefficients up to the stall has been plotted in figure 23. This curve was obtained by cross-plotting for $C_m = 0$ the results of the ailavator-effectiveness tests given in figures 16 to 19. The results of figure 23 show that the airplane with propeller removed can be trimmed by means of the unit horizontal tail for all lift coefficients up to $C_L = 0.72$.

As an indication of the stick-free longitudinal stability characteristics of the airplane, the variation of C_m with C_L for $C_{h_a} = 0$ is presented in figure 24 for the complete model configuration. Although the data are rather limited, these results indicate that the stick-free stability will be erratic over most of the lift coefficient range investigated and will be unstable at very low lift coefficients (below about 0.1).

Effect of unit horizontal tail.- The effect of the unit horizontal tail on the aerodynamic characteristics of the basic model are shown in figure 25. The horizontal tail, at zero incidence, contributes an increment of about 0.18 to the maximum lift coefficient of the model. As shown by the pitching-moment curve the model with the horizontal tail removed is unstable between $\alpha = 0°$ and $12°$ and becomes stable at angles of attack greater than $12°$. The contribution of the unit horizontal tail to the longitudinal stability of the basic model is shown in figure 26 by the increment in model pitching-moment coefficient provided by the tail

plotted against angle of attack. The value of $\partial\Delta C_{m_t}/\partial\alpha$ is about -0.0059 between $\alpha = 0^{\circ}$ and 12° and decreases to about -0.0022 for angles of attack greater than 12°. This decrease in slope at the higher angles of attack is probably due to the stalling of the horizontal tail.

Ailavator-tab effectiveness.- The results of the tab tests, which are presented in figures 27 to 30, show the effects of tab deflection on the variations of C_{h_a}, C_m, C_L, and C_D with ailavator deflection for three angles of attack ($\alpha = -0.6^{\circ}$, 11.3°, 23.2°). The tab hinge-moment parameter $\partial C_{h_a}/\partial\delta_{a_T}$ remains essentially constant with ailavator deflection but increases negatively from -0.0033 at $\alpha = -0.6^{\circ}$ to -0.0045 at $\alpha = 23.2^{\circ}$. (See fig. 27.) A decrease in the model pitching-moment coefficient of about -0.0005 per degree change in tab deflection was measured. (See fig. 28.) This decrease in pitching-moment coefficient did not change appreciably with angle of attack or ailavator deflection. The results of figures 29 and 30 show that tab deflection had no appreciable effect on the lift and the drag of the model.

Stability-flap effectiveness.- The results of the flap tests presented in figures 31 to 34 show the variations with flap deflection of C_m, C_{h_f}, C_L, and C_D. The main purpose of the stability flap is to trim out the adverse or stalling pitching moment due to propeller operation. The flap effectiveness $\partial C_m/\partial\delta_f$ increased negatively with angle of attack up to $\alpha = 23.2^{\circ}$ and thereafter remained approximately constant until the stall. (See fig. 31.) A decrease in the basic-model pitching-moment coefficient of about -0.0017 per degree change in flap deflection was measured at $\alpha = -0.6^{\circ}$ and this value increased to about -0.0026 at $\alpha = 23.2^{\circ}$. The value of $\partial C_{h_f}/\partial\delta_f$ at small flap deflections, increased with angle of attack (fig. 32) from about zero at $\alpha = -0.6^{\circ}$ to about -0.0019 at $\alpha = 35.2^{\circ}$. The value of $\partial C_{h_f}/\partial\delta_f$ increased rapidly, in the negative direction, for large positive flap deflections. The effects of flap deflection on the lift coefficient were comparatively small. A maximum increase in lift coefficient of only 0.12 (at $\alpha = 11.3^{\circ}$) was measured for full positive flap deflection. (See fig. 33.)

Aileron effectiveness.- The results of the aileron tests are given in figures 35 and 36 for angles of attack of -0.6°, 11.3°, and 23.2°. The aileron effectiveness $\partial C_l/\partial\delta_{a_R}$ with only one ailavator deflected increased slightly from about -0.0018 at $\alpha = -0.6^{\circ}$ to about -0.0022 at $\alpha = 23.2^{\circ}$. (See fig. 35.) The values of $\partial C_{h_a}/\partial\delta_{a_R}$ were small and about zero for conditions other than those in which it appears that the ailavator was stalled. At $\alpha = -0.6^{\circ}$ it appears that the control surface might be overbalanced.

Rudder effectiveness.- The results of the rudder tests are given in figures 37 and 38 for angles of attack of -0.6°, 11.3°, and 23.2°. The rudder parameters $\partial C_n/\partial\delta_r$, $\partial C_Y/\partial\delta_r$, and $\partial C_{h_r}/\partial\delta_r$ increased with angle

of attack; so that for an angle-of-attack range of -0.6° to 23.2°, $\partial C_n / \partial \delta_r$ increased slightly from about -0.0010 to about -0.0012, $\partial C_Y / \partial \delta_r$ increased from about 0.0019 to about 0.0026, and $\partial C_{h_r} / \partial \delta_r$ increased from about -0.0042 to about -0.0078. Rudder deflection appears to have a large effect on the rolling moment of the model. (See fig. 37.) An average change in the model rolling-moment coefficient of about -0.0007 per degree change in rudder deflection was measured.

Results with Propellers Operating

<u>Propulsive characteristics</u>.- The design of the airplane was based on the premise that the aerodynamic characteristics of the low-aspect-ratio wing could approach those of a high-aspect-ratio wing by the addition of large-diameter propellers located at the wing tips and rotating in opposite direction to the tip vortices. In this manner the energy of the tip vorticity would be partially counteracted by the rotational energy of the propeller slipstream. With the propellers rotating upward in the center, the lift vector is inclined forward because of the added upwash due to slipstream rotation and thus the induced drag of the wing is decreased.

For these tests, the effect of propeller operation have been determined by an evaluation of the propulsive efficiency, expressed $\eta = \dfrac{(D_u - D_{R_u})V}{2P}$ in which $\dfrac{D_u - D_{R_u}}{2}$ is the propulsive thrust per propeller and D_u and D_{R_u} are the propellers-removed drag and the resultant drag with propellers operating (measured at the same lift coefficient), respectively. The propulsive efficiency thus includes any effect of propeller operation on the lift and the drag. The results of tests made to determine the propulsive efficiency of the model at angles of attack of -0.5°, 5.4°, and 11.4° for $\beta = 20°$ and at -0.6°, 5.3°, and 11.3° for $\beta = 30°$ are presented in figure 39. The peak propulsive efficiency of the present propeller installation on the airplane at $\alpha = -0.6°$ and $\beta = 30°$ is 0.75. (See fig. 39(c).)

The results of figure 39 show an increase in the effective thrust coefficient and propulsive efficiency with angle of attack, as expected. At zero angle of attack, the lift coefficient and, therefore, the induced drag are approximately zero and the effect of the slipstream rotation will be small. As the angle of attack is increased, however, the down flow at the wing due to the tip vorticity is partially offset by the up flow due to the slipstream rotation of the propeller; also the propellers begin to contribute a considerable vertical force that increases the total lift. These effects both tend to reduce the induced drag of the wing and to increase the propulsive efficiency of the airplane-propellers combination. Further increases in angle of attack and power result in the propellers carrying directly more and more of the total lift.

The results of tests made to determine the effects of direction of propeller rotation on the propulsive characteristics of the model are given in figure 40 for $\beta = 20^\circ$ and $\beta = 30^\circ$. The tests were made at negative as well as positive angles of attack for the same propeller rotation inasmuch as at negative angles of attack the rotation of the propeller slipstream with respect to the rotation of the tip vortices is effectively reversed since the wing is symmetrical. The results of the tests show 7 percent greater peak propulsive efficiency at the positive angle of attack for $\beta = 20^\circ$ at $C_L \cong 0.67$ and 20 percent greater for $\beta = 30^\circ$ at $C_L \cong 0.74$. The larger increase for $\beta = 30^\circ$ is probably because the rotation of the slipstream is greater for $\beta = 30^\circ$ than for $\beta = 20^\circ$ over the V/nD range investigated thus counteracting a greater percentage of the induced drag.

Static-thrust tests.- The results of tests made to determine the static thrust obtainable with several propeller blade angles are presented in figure 41. The propeller blade angle for maximum static thrust can be obtained from the curve of C_{T_e}/C_Q plotted against propeller blade angle. The optimum propeller blade angle for static thrust is 11.5° where the ratio C_{T_e}/C_Q is a maximum $\left(\dfrac{C_{T_e}}{C_Q} = 17.5 \right)$.

Effects of propeller operation on lift.- The effects of propeller operation on the lift of the model are presented in figure 42 at angles of attack ranging from about 0° to 30°. At angles of attack of -0.5° and -0.6° for propeller blade angles of 20° and 30°, respectively, increases in C_L amounting to between 0.2 and 0.3 were measured for the V/nD ranges investigated. This change in lift coefficient is caused principally by the change in the local angles of attack of the wing induced by slipstream rotation.

As the angle of attack is increased the change in lift coefficient at a given V/nD increases. Calculations showed that about one-third to one-half of the total increase in lift due to propeller operation at the high angles of attack results from the lift component of the propeller resultant force. Most of the remaining increase is attributed to the increased slipstream velocity over the wing.

The results of tests made of the basic model configuration for angles of attack of from 3° to 84° with the propellers operating at blade angles of 10°, 11.5°, 14°, 20°, and 30° are given in figure 43. Additional data for a propeller blade angle of 20° with the model mounted on the wing-tip support are given in figure 44. These curves give the variations of C_L, C_{D_R}, and V/nD with Q_c which were used in the determination of the maximum lift coefficient of the airplane with the propellers operating. The tests at very high angles of attack were made only with a propeller blade angle of 11.5°, inasmuch as preliminary check tests indicated this setting to be optimum for the static-thrust condition.

Curves for the airplane of Q_c against C_L for both full-power operation (1200 bhp at 1085 rpm) and 115 percent full-power operation (1380 bhp at 1085 rpm) are included in figures 43(a), 43(f), and 43(i) in order to determine points of simulation of airplane Q_c from model test data. The intersection of the airplane curve with the model data represents this simulation for a particular blade angle as shown by the ticks in figures 43(a), 43(f), and 43(i). The points of intersection determined from figures 43 and 44 will be used later in the determination of the maximum lift coefficient of the airplane with propellers operating.

Inasmuch as the effects of propeller operation on the lift of the subject airplane are large, especially at the higher angles of attack, the determination of the propellers-operating lift curve required the duplication of the correct blade angle and advance ratio in addition to the torque coefficient. The process used in the determination of the propellers-operating lift curve for full-power operation at sea level is as follows: From the intersections of the airplane curve with the model curves of figures 43 and 44, curves of α against C_L and V/nD against C_L were plotted for the several blade angles as shown in figure 45. Superimposed on these constant-blade-angle curves, which duplicate the required airplane torque coefficients, is the variation of V/nD with C_L of the airplane for full-power operation. The intersection of the model V/nD against C_L curve for a particular blade angle with the airplane V/nD against C_L curve give a point at which airplane torque coefficient, blade angle, and V/nD are duplicated. These intersections are noted by the ticks in figure 45. The airplane lift curve for full-power operation can be traced by a line through the ticks on the α against C_L curves of figure 45.

The peaks of the α against C_L curves of figure 45 determine the maximum lift coefficient obtainable at a particular blade angle for full-power operation. The simulation point for $\beta = 14°$ occurs at the peak of the lift curve; therefore, the maximum lift coefficient for full-power operation should be 1.90 at $\alpha = 29.2°$ and corresponds to a minimum flight speed of about 90 miles per hour.

The indicated higher maximum lift coefficient of the airplane for a propeller blade angle of 11.5° (fig. 45) was not attained with the present rated power (1200 bhp at 1085 rpm) and weight (16,750 lb) of the airplane. A few calculations were made to determine the required changes in the airplane basic parameters that would enable the airplane to fly on the $\beta = 11.5°$ curve. It was first desired to change the airplane weight while maintaining the normal rated power of the airplane. Calculations showed that a flight-simulation point for $\beta = 11.5°$ at $C_L = 3.0$ (fig. 46) at $\alpha = 46.7°$ could be attained by decreasing the airplane weight by 14.2 percent. This lift coefficient corresponded to a minimum speed of about 72 miles per hour. It was next desired to make changes in both the power and weight. As shown in figure 46 the maximum lift coefficient could be increased to 8.9 at $\alpha = 51.5°$ for $\beta = 11.5°$ by increasing the power 15 percent (1380 bhp at 1085 rpm) and by decreasing the weight 23.6 percent. A lift coefficient of 8.9 corresponds to a minimum flight speed of about 42 miles per hour.

In order to obtain additional information concerning the performance of the airplane in the very high angle-of-attack range ($\alpha_u = 42^\circ$ to 72°), an analysis was made of the power that would be required to maintain unaccelerated level flight (as defined by a point where $C_{D_R} = 0$). Curves showing the variation of C_{D_R}, Q_c, α, and V/nD with C_L for $\beta = 11.5^\circ$ in the region of $C_{D_R} = 0$ only are presented in figure 47. (Some of these data are a repetition of the data of fig. 43.) Calculations of the power required were made based on the values obtained at $C_{D_R} = 0$, and the variation of horsepower required (per propeller), C_L, V/nD, and α with forward-flight speed V calculated on this basis are shown in figure 48. For the speed range investigated the horsepower required per propeller increases from about 1290 horsepower at $C_L = 2.40$ to 1690 horsepower at $C_L = 10.75$. (See fig. 48.) This increase in horsepower is from 8 to 41 percent greater than the normal rated horsepower of the airplane. As shown in figure 48, the minimum forward-flight speed of the airplane (for normal gross weight) for level flight is about 38 miles per hour, based on the lift coefficient of 10.75 at $\alpha = 69^\circ$. Calculations indicated that an increase in the propeller-rotational speed of about 10 percent would be required throughout the speed range investigated. The need for this increase in propeller-rotational speed could probably be eliminated by changing the propeller blade angle slightly.

CONCLUSIONS

The results of a preliminary investigation of a $\frac{1}{3}$-scale model of a convertible-type airplane in the Langley full-scale tunnel showed the following:

1. Early air-flow separation at the wing center section was caused by mutual interference effects of the engine-air-duct installations and an upright canopy on the wing. As a result, the comparatively low value of maximum lift coefficient of 0.97 was measured for the complete model configuration with the propellers removed. With the engine air ducts and canopy removed, a maximum lift coefficient of 1.31 was measured.

2. Installing extended spinners in the engine air ducts and extending the canopy afterbody increased the maximum lift coefficient of the model with the propellers removed by 0.08 and 0.06, respectively.

3. The model with the propellers removed (normal center-of-gravity location) has a positive static margin, stick fixed, varying from 5 to 13 percent of the mean aerodynamic chord throughout the unstalled range of lift coefficients.

4. The unit horizontal tail is sufficiently powerful to trim the airplane with the propellers removed throughout the unstalled range of lift coefficients.

5. The effect of the unit horizontal tail on the airplane longitudinal stability, as determined by the slope of the curve of tail pitching-moment coefficient against angle of attack $\partial\Delta C_{mt}/\partial\alpha$ decreased from about -0.0059 at angles of attack up to 12° to about -0.0022 for angles of attack greater than 12°.

6. The peak propulsive efficiency was 7 percent greater at $\beta = 20^{\circ}$ at $C_L \cong 0.67$ and 20 percent greater at $\beta = 30^{\circ}$ at $C_L \cong 0.74$ with the propellers rotating upward in the center than with the propellers rotating downward in the center.

7. Propeller operation caused large changes in the lift of the model, especially at the higher angles of attack. Calculations showed that about one-third to one-half of the total increase in lift due to propeller operation at the high angles of attack was due to the vertical component of the thrust of the propellers.

8. Based on a maximum lift coefficient of 1.90, indications are that the minimum forward-flight speed of the airplane having a gross weight of 16,750 pounds for full-power operation at sea level (1200 bhp at 1085 rpm) will be about 90 miles per hour. Decreasing the airplane weight and increasing the power decreased this value of minimum speed, such that for 15 percent greater power and a 23.6 percent decrease in weight, the minimum speed was about 42 miles per hour at $\alpha = 51.5^{\circ}$. The results did not indicate any limit to the minimum speed provided the necessary changes in power and weight could be made.

Langley Aeronautical Laboratory
    National Advisory Committee for Aeronautics
        Langley Air Force Base, Va.

<div align="center">REFERENCES</div>

1. Glauert, H.: Wind-Tunnel Interference on Aerofoils. R. & M. 1470, British A.R.C., 1932.

2. DeFrance, Smith J.: The N.A.C.A. Full-Scale Wind Tunnel. NACA Rep. 459, 1933.

3. Schuldenfrei, Marvin: Some Notes on the Determination of the Stick-Fixed Neutral Point from Wind-Tunnel Data. NACA RB 3I20, 1943.

TABLE I

MODEL CONTROL—SURFACE DATA

	Unit horizontal tail	Vertical tail	Rudder	Flap
Area, sq ft	2.79	1.58	[a]0.59	0.84
Span, ft	2.77	1.43	1.43	1.81
Root—mean—square chord, ft	1.01	--------	[b]0.38	[b]0.57
Aspect ratio	2.75	1.29	----------	3.91
Control deflection, deg	55 up 25 down	5 right, 10 left	30 right, 30 left	10 up, 30 down
Trim—tab area, sq ft	0.68	--------	----------	--------

[a]Area aft of hinge line.
[b]Chord aft of hinge line.

NACA
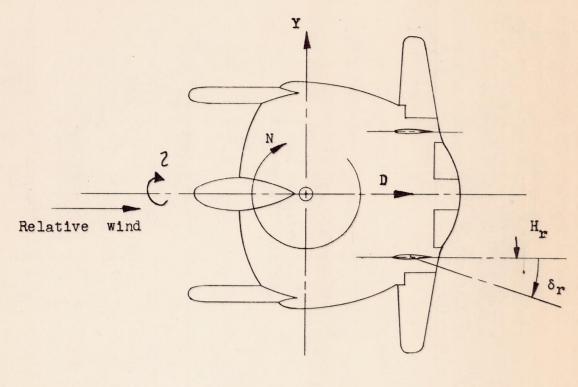
TABLE II

INDEX OF MAXIMUM LIFT RESULTS

PROPELLERS REMOVED

No.	Model configuration	$C_{L_{max}}$	Reference figure
1	Complete Model	0.97	3, 12
2	Same as 1 except canopy open	.98	-----------
3	Same as 2 except fillets installed	.96	-----------
4	Same as 1 except engine-air-duct inlets sealed with bulbous fairings	1.05	5, 13
5	Same as 4 except extended canopy afterbody installed	1.11	6, 13
6	Same as 1 except engine-air outlets unsealed	.96	-----------
7	Same as 1 except engine-air ducts removed	1.19	13
8	Same as 3 except extended spinners installed	1.04	7, 8, 9, 13
9	Same as 8 except upright canopy and fillets removed	1.11	10, 13
10	Basic model	1.31	4, 14

NACA
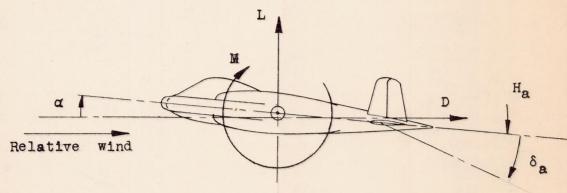
Figure 1.— System of axes and control-surface hinge moments and
deflections. Positive values of forces, moments, and angles
are indicated by arrows. Positive values of tab deflections
are in the same directions as the positive values for the
control surfaces to which the tabs are attached.

1.806

Ailavators

1.999

2.773

Stability flaps

0° Incidence

¢ hinge line, 0.257 chord

1.364

7.77

7.77

Geometric Characteristics

Aspect ratio   1.27

Areas   sq ft
Wing (including stability flap)...... 47.444
Stability flaps (two)............... 1.671
Unit horizontal tail (two ailavators)..5.578
Vertical tails (two)................ 3.158
Horizontal tail tab (one)......... 0.338

Lengths   ft
Span   7.777
Mean aerodynamic chord   6.611

Airfoil sections
Wing .... NACA 0016
Horizontal tail
        Root........ NACA 0015
        Tip   NACA 0009
Vertical tail..12-percent thick, symmetrical

**NATIONAL ADVISORY
COMMITTEE FOR AERONAUTICS.**

5.33

1.444

1.583

C.G, 0.263c̄

0° Incidence

Thrust axis and chord line

Figure 2.— General arrangement and geometric characteristics of a $\frac{1}{3}$—scale model of a convertible—type airplane. (All dimensions are given in ft.)
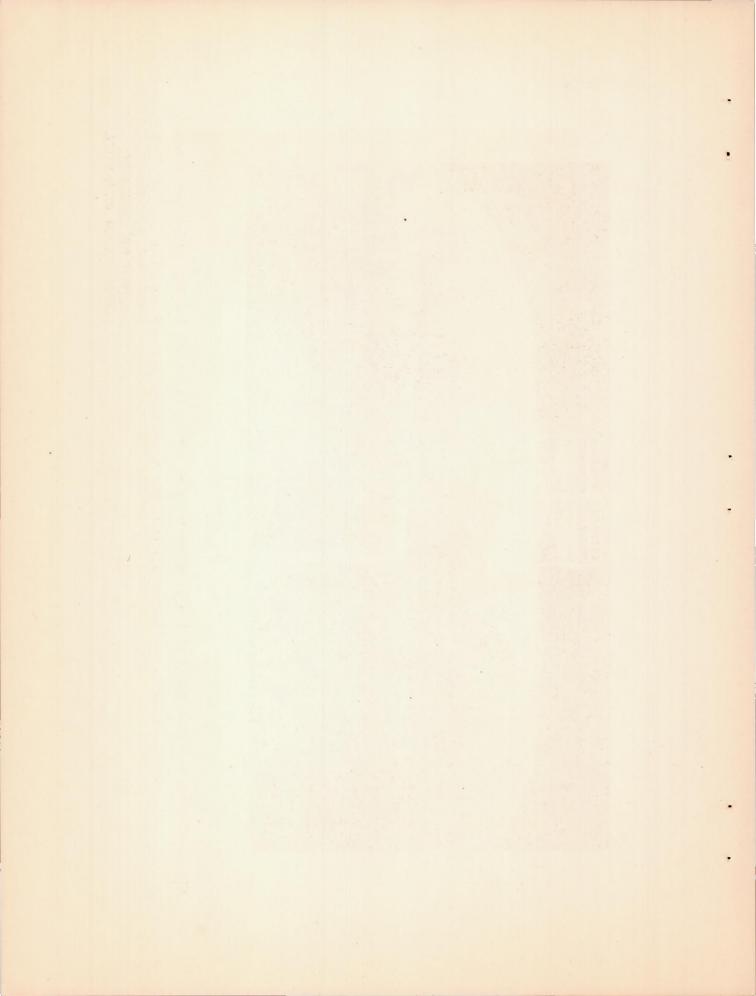
Figure 3.— The $\frac{1}{3}$—scale model of the airplane mounted for tests in the Langley full—scale tunnel. Model in complete configuration; propellers removed; wing—tip support.

NATIONAL ADVISORY
COMMITTEE FOR AERONAUTICS.
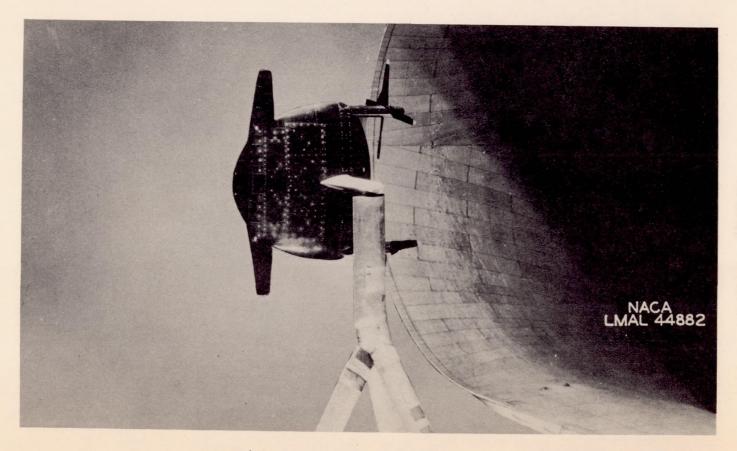
(a) Front view.

Figure 4.— The $\frac{1}{3}$—scale model of the airplane mounted for tests in the Langley full—scale tunnel. Model in basic configuration; semispan support; propellers installed.

NATIONAL ADVISORY
COMMITTEE FOR AERONAUTICS.
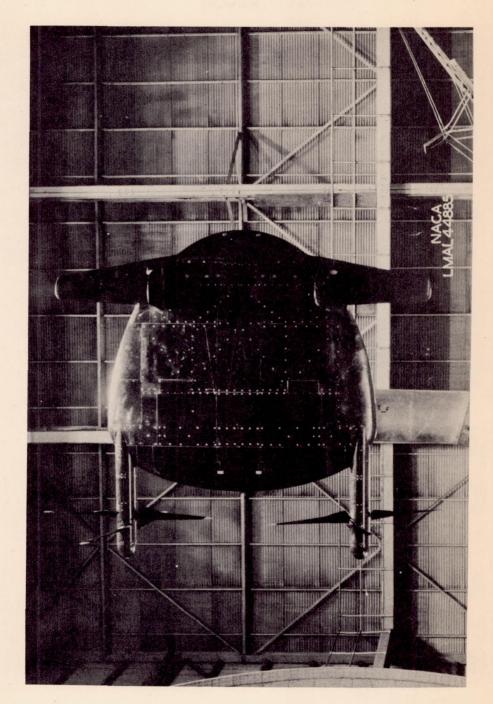
(b) Three-quarter rear view.

Figure 4.— Continued.
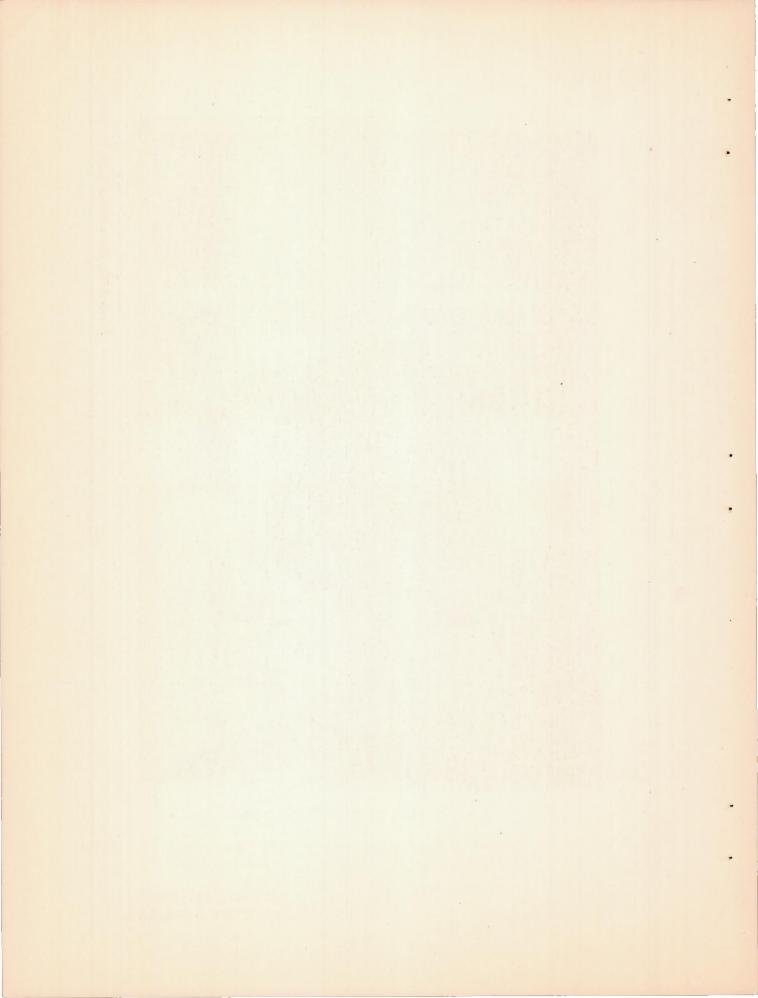
NATIONAL ADVISORY
COMMITTEE FOR AERONAUTICS.

(c) Side view.

Figure 4.— Concluded.

NATIONAL ADVISORY
COMMITTEE FOR AERONAUTICS.

(a) Plan view.

(b) Three-quarter front view.

Figure 5.— Details of configuration 4 showing engine—air—duct inlets
sealed with bulbous fairings. Propellers removed.

NATIONAL ADVISORY
COMMITTEE FOR AERONAUTICS.
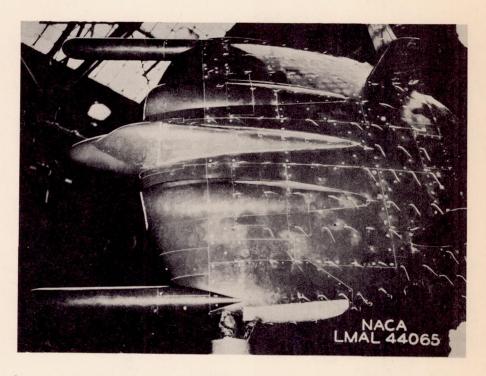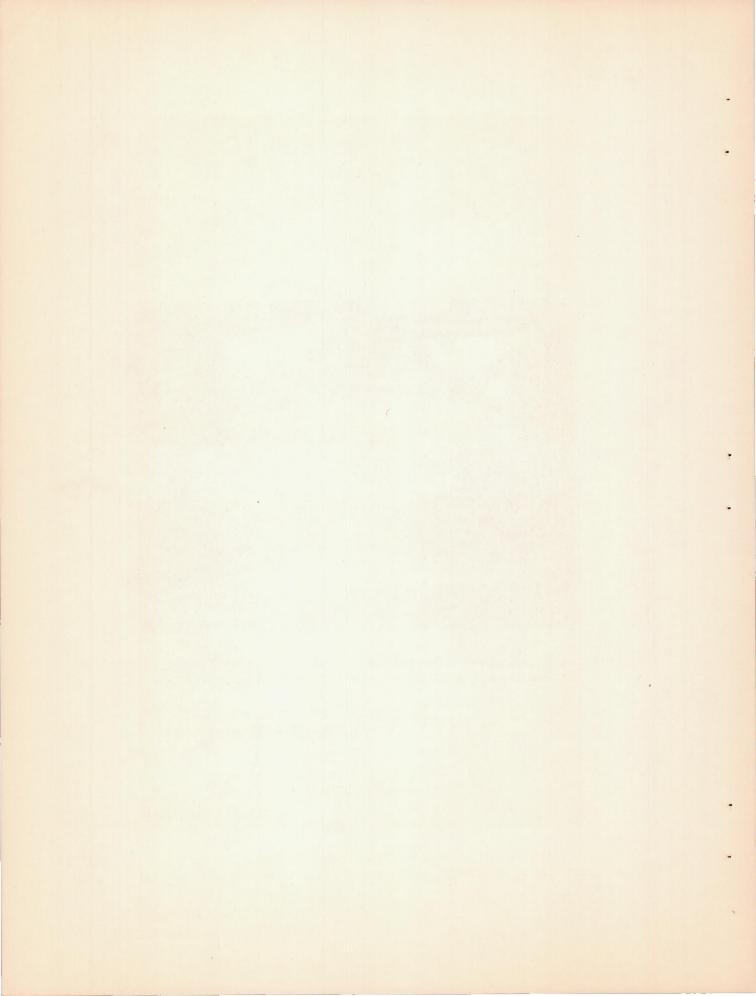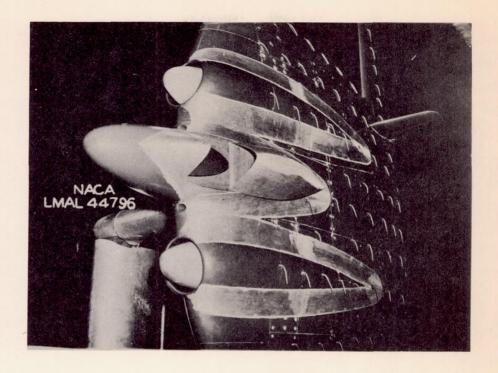
Figure 6.— Configuration 5 showing extended canopy afterbody installed. Engine-air-duct inlets sealed; propellers removed.

NATIONAL ADVISORY
COMMITTEE FOR AERONAUTICS.
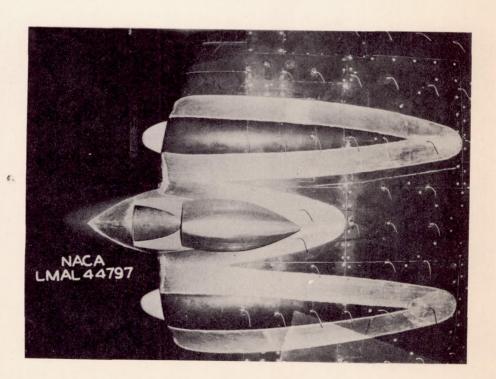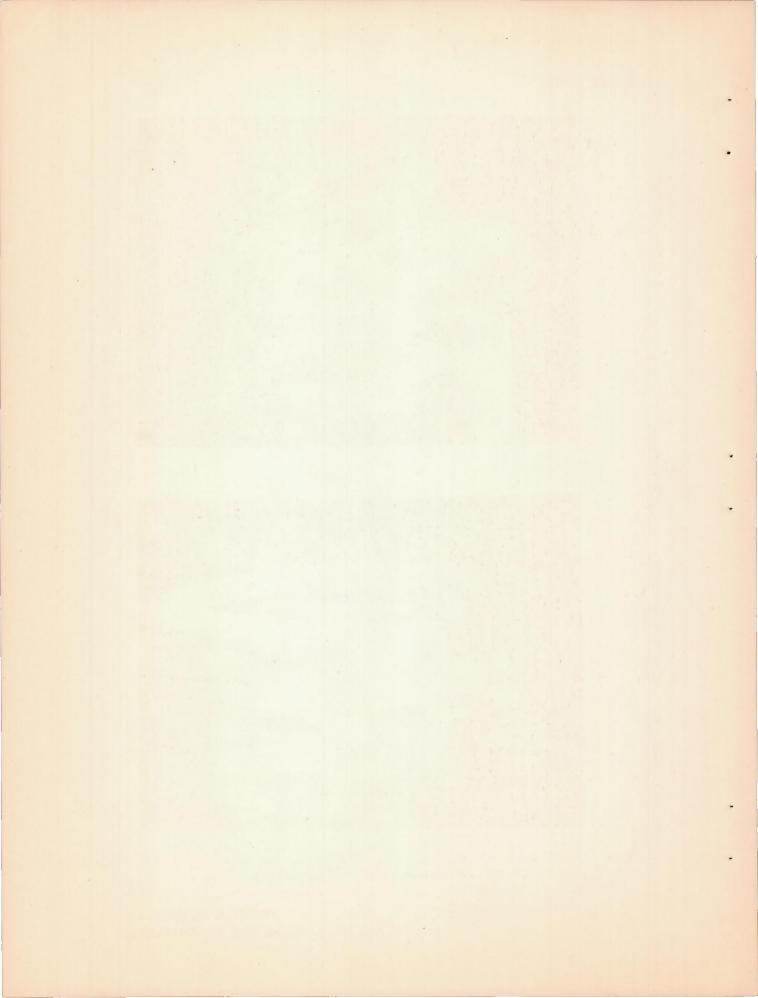
Figure 7.— Details of configuration 8 showing extended spinners in engine–
air-ducts, fillets, and open canopy. Propellers removed.

NATIONAL ADVISORY
COMMITTEE FOR AERONAUTICS.

Resistance plate

Wing leading edge

Plan view

———— Extended spinner
– – – – Original spinner

Side view
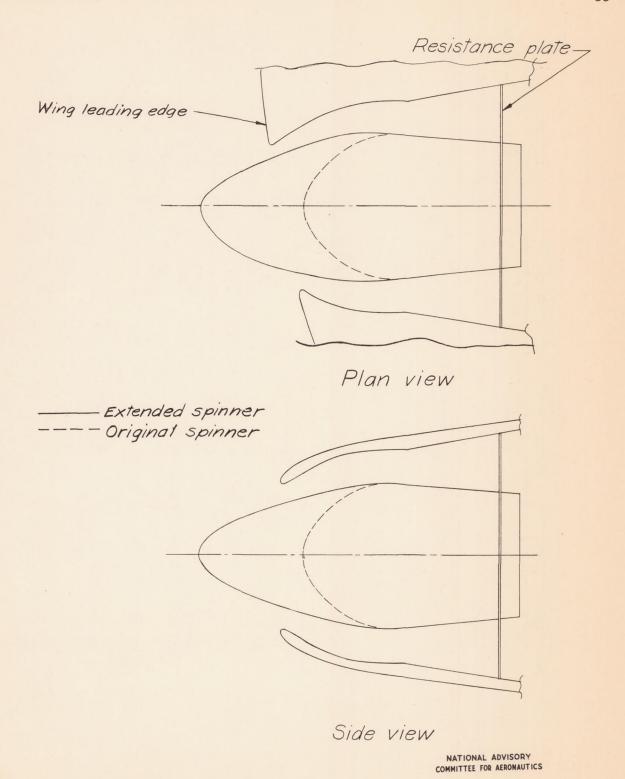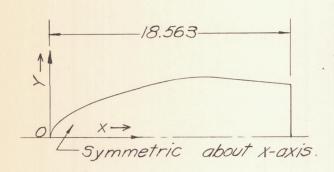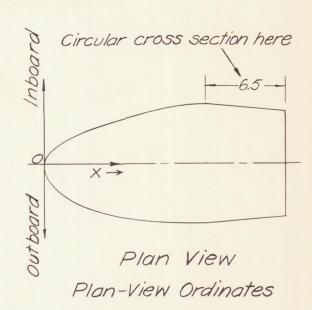
Figure 8.— Arrangement of engine-air-duct installation at wing leading
edge. Spinners do not revolve in ducts.

18.563

Y

O   X →

Symmetric about x-axis.

Circular cross section here

Inboard

Outboard

6.5

O   X →

Side View

Side-View Ordinates

Plan View

Plan-View Ordinates

X	Y
0.06	0.38
.13	.59
.25	.84
.50	1.25
.75	1.53
1.00	1.76
1.50	2.06
2.00	2.31
4.00	3.05
6.00	3.63
8.00	4.11
9.00	4.59
10.00	4.42
11.00	4.50
12.00	4.50
15.00	4.28
18.563	4.00

X	Outboard	Inboard
0.00	0.25	----
.06	.66	0.38
.13	.88	.58
.25	1.16	.84
.50	1.56	1.19
.75	1.88	1.41
1.00	2.09	1.61
1.50	2.44	1.91
2.00	2.73	2.16
4.00	3.61	3.05
6.00	4.16	3.81
8.00	4.53	4.38
9.00	4.59	4.50
10.00	4.61	4.55
11.00	4.58	4.55
12.00	4.51	4.50
15.00	4.28	4.28
18.563	4.00	4.00

NATIONAL ADVISORY
COMMITTEE FOR AERONAUTICS

Figure 9.— Details of the extended-spinner installation. (All dimensions
are given in inches.)
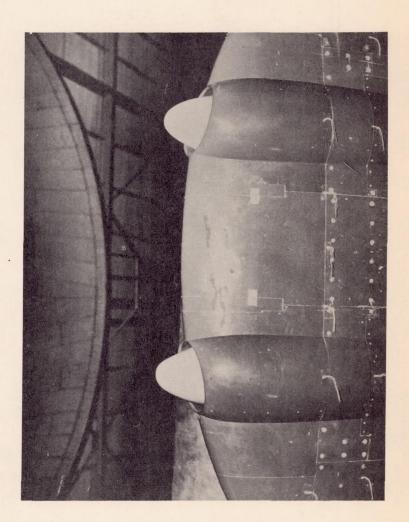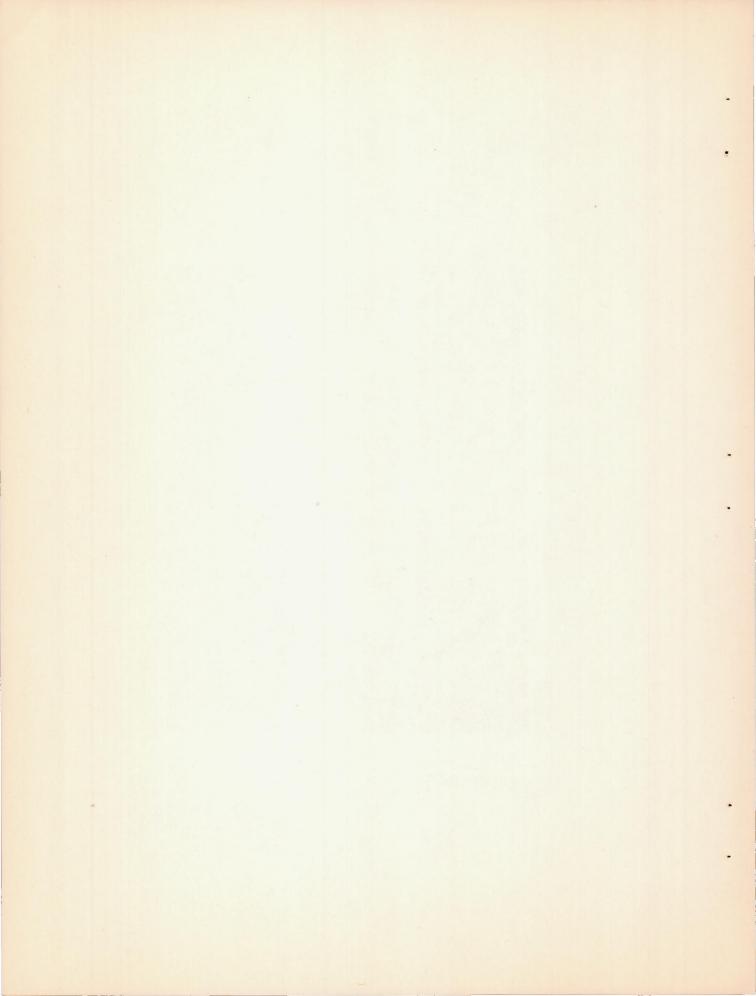
Figure 10.— Configuration 9 showing canopy installation removed. Extended spinners installed; propellers removed.

NATIONAL ADVISORY
COMMITTEE FOR AERONAUTICS.
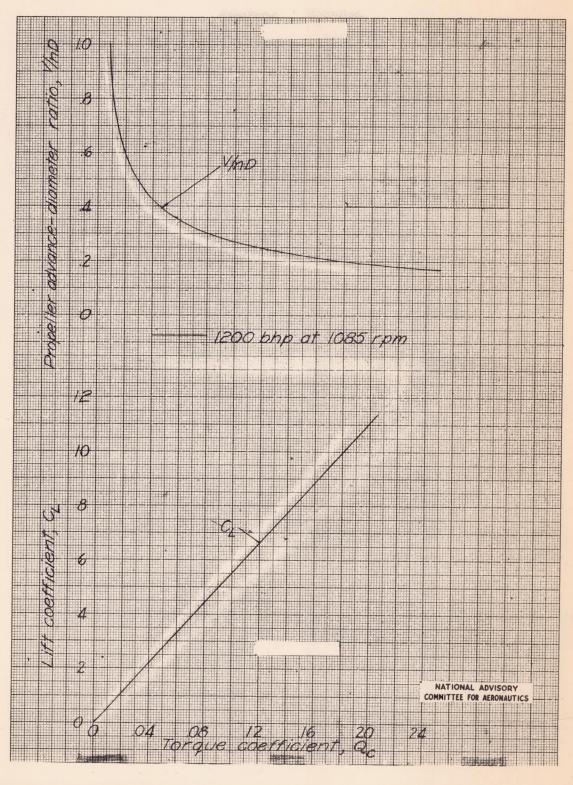
Figure 11.— Variation of C_L and V/nD with Q_c of the airplane for full—power operation at sea level.
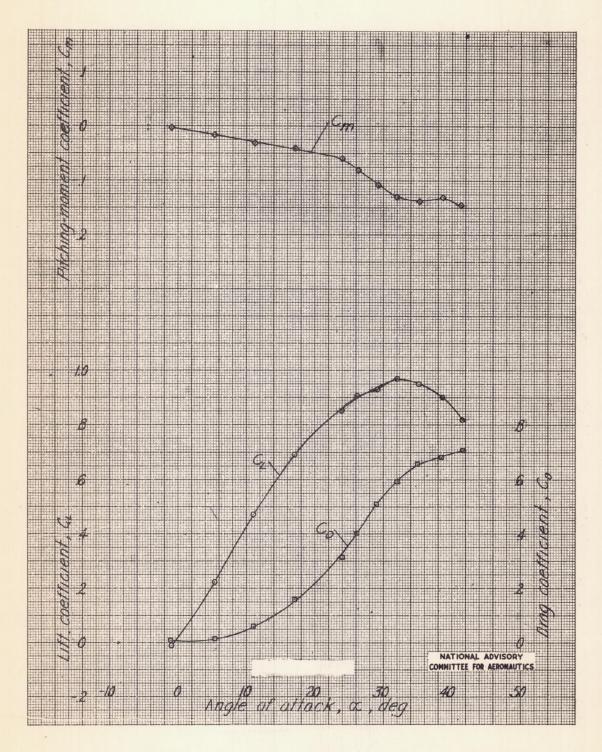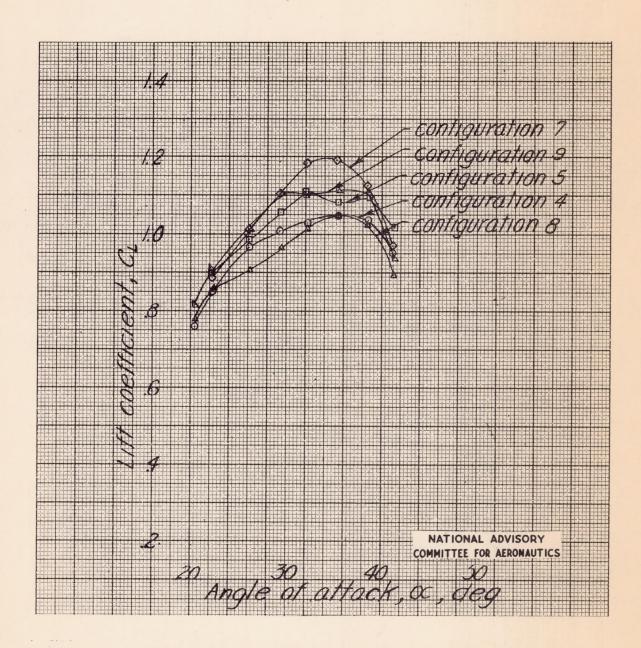
Figure 12.— Variation of C_L, C_D, and C_m with α of a $\frac{1}{3}$—scale model of the airplane. Complete model configuration; propellers removed.

Figure 13.— Comparison of maximum lift coefficients obtained with five
model configurations. (See table II.) Propellers removed.
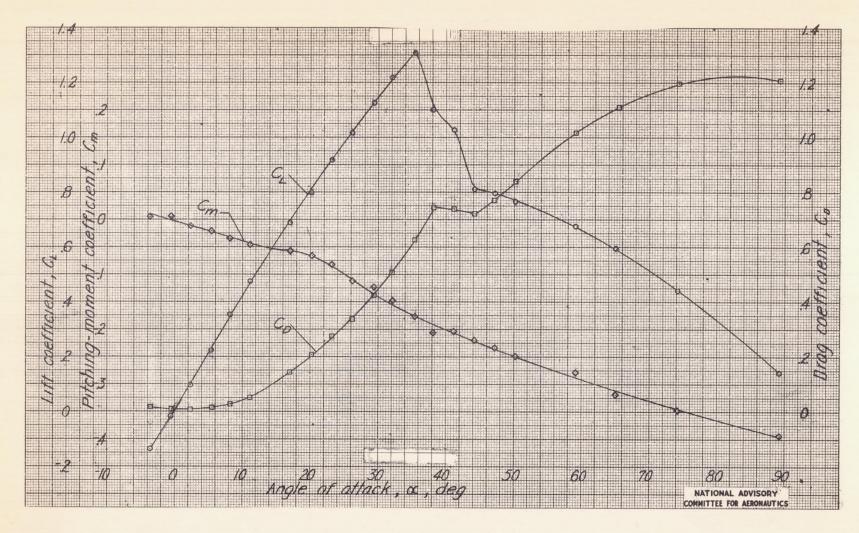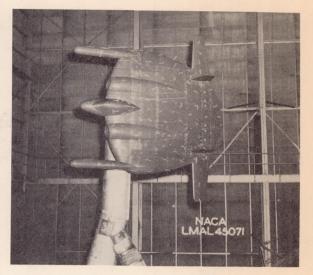
Figure 14.— Variation of C_L, C_D, and C_m with α of a $\frac{1}{3}$-scale model of the airplane. Basic model configuration; propellers removed.

$a = 25.4°; \quad C_L = 0.91$

$a = 29.2°; \quad C_L = 0.93$

$a = 32.2°; \quad C_L = 0.97$

$a = 35.2°; \quad C_L = 0.95$
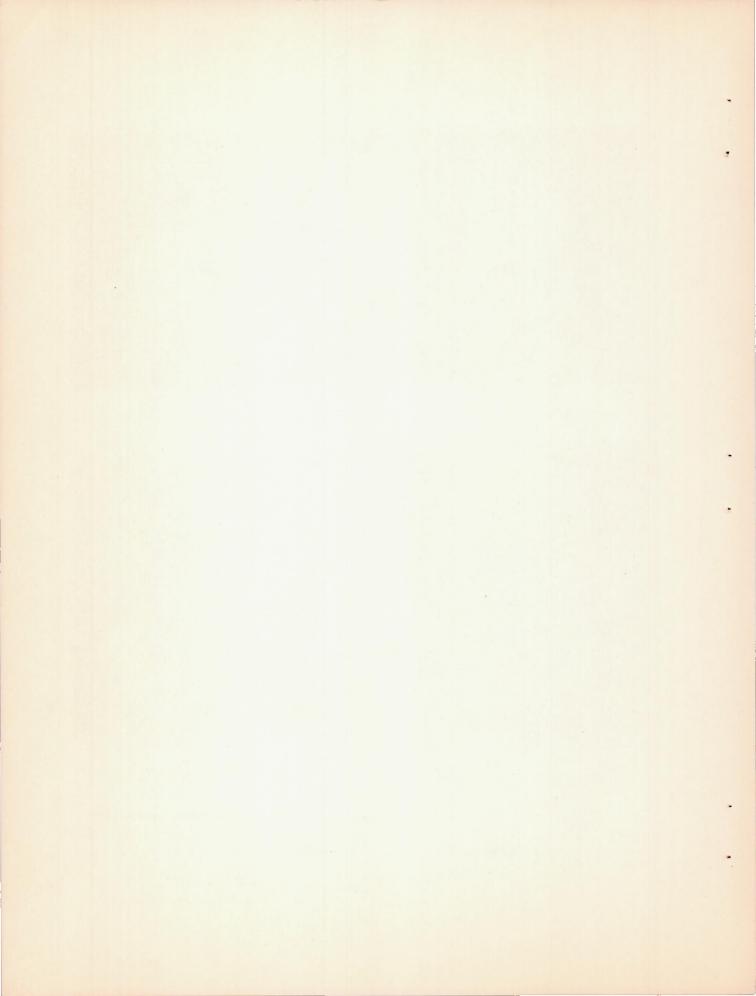
(a) Configuration 1.
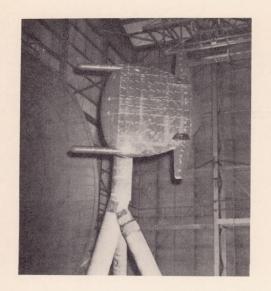
Figure 15.— Tuft observations on the $\frac{1}{3}$-scale model of the airplane.
Propellers removed.
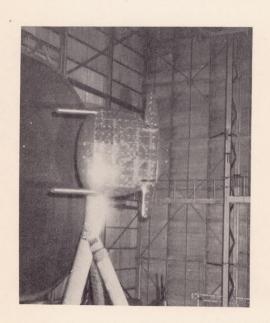
NATIONAL ADVISORY
COMMITTEE FOR AERONAUTICS.

$a = 26.3°; \ C_L = 1.01$

$a = 29.3°; \ C_L = 1.12$

$a = 35.3°; \ C_L = 1.31$
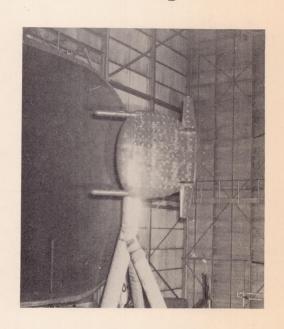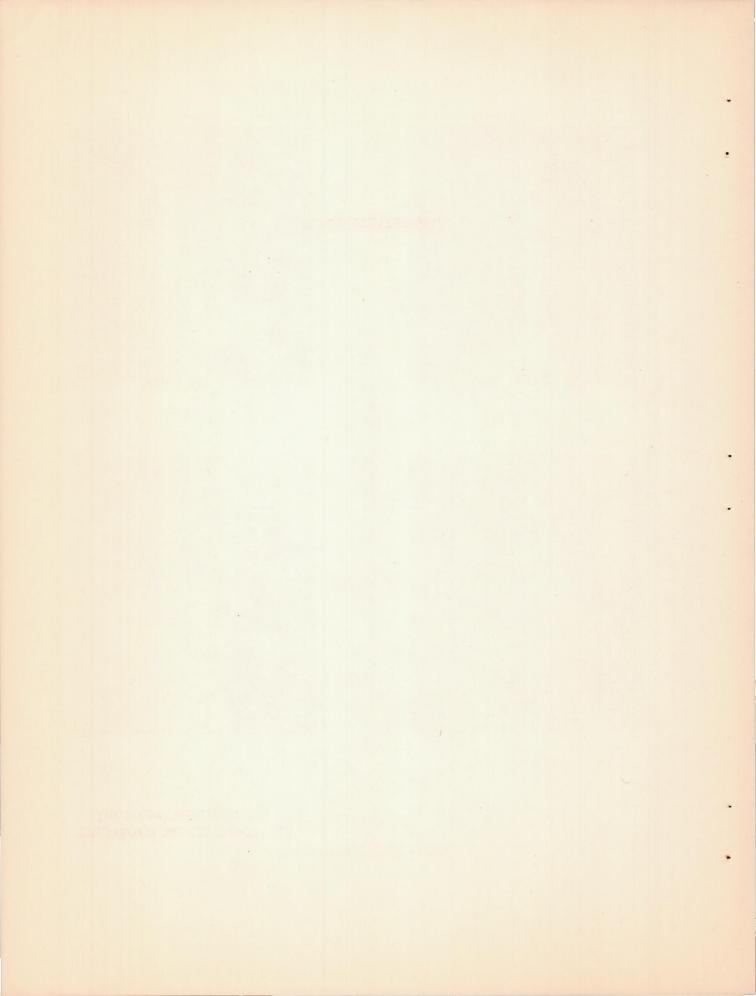
$a = 44.3°; \ C_L = 0.81$

(b) Configuration 10.

**NATIONAL ADVISORY
COMMITTEE FOR AERONAUTICS.**

Figure 15.— Concluded.
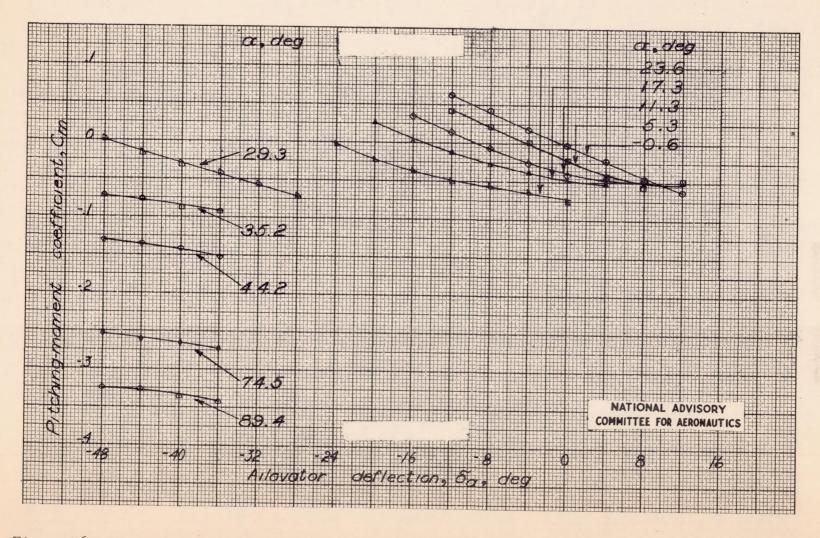
Figure 16.— Variation of pitching-moment coefficient with ailavator deflection. Model in complete configuration; $\delta_{a_{T_L}} = \delta_{a_{T_R}} = 0^\circ$; $\delta_r = 0^\circ$; propellers removed; $\delta_f = 0^\circ$.
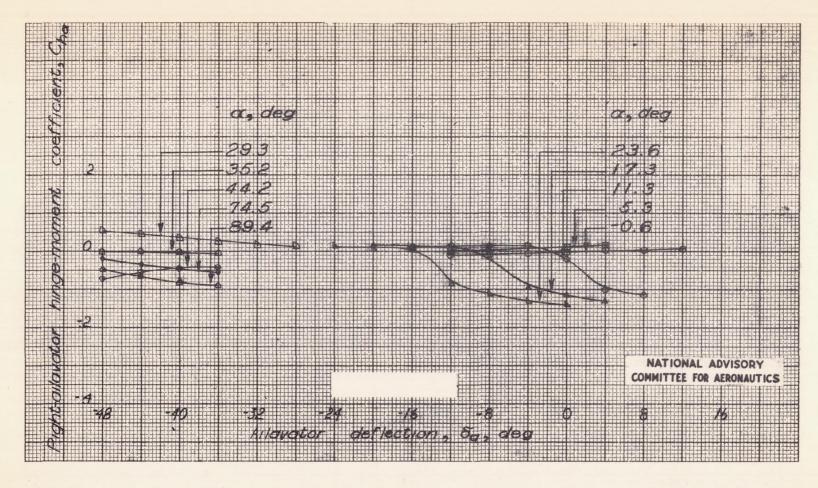
Figure 17.— Variation of right—ailavator hinge—moment coefficient with ailavator deflection.   Model in complete configuration; $\delta_{a_{T_L}} = \delta_{a_{T_R}} = 0°$; $\delta_r = 0°$; propellers removed; $\delta_f = 0°$.
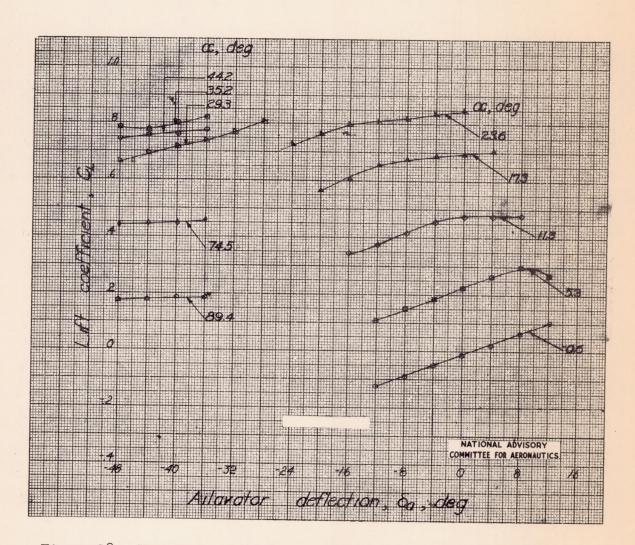
Figure 18.— Variation of lift coefficient with ailavator deflection. Model in complete configuration; $\delta_{a_{T_L}} = \delta_{a_{T_R}} = 0^o$; $\delta_r = 0^o$; $\delta_f = 0^o$; propellers removed.
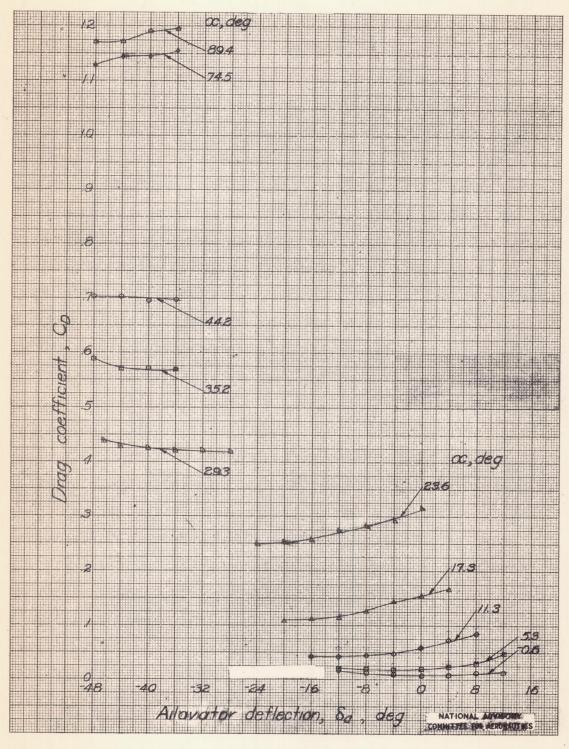
Figure 19.— Variation of drag coefficient with ailavator deflection. Model in complete configuration; $\delta_{a_{T_L}} = \delta_{a_{T_R}} = 0°$; $\delta_r = 0°$;

$\delta_f = 0°$; propellers removed.
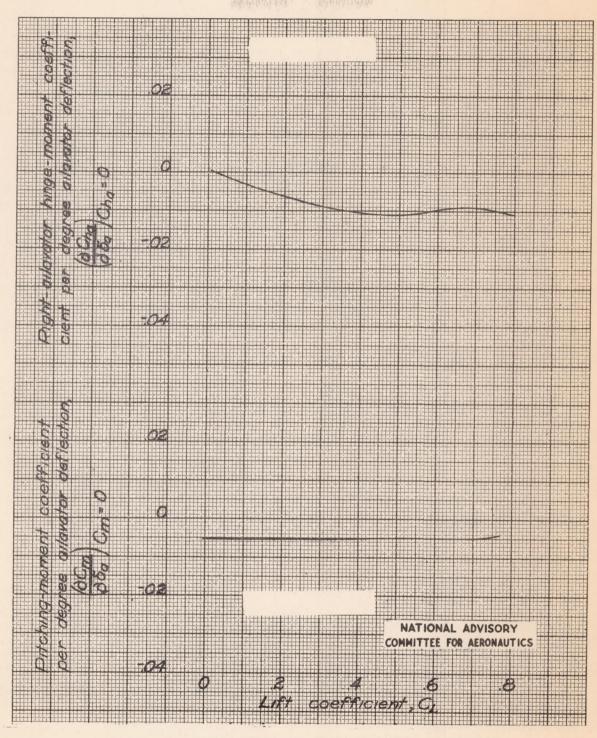
Figure 20.— Variation of $\left(\dfrac{\partial C_m}{\partial \delta_a}\right)_{C_m\,=\,0}$ and $\left(\dfrac{\partial C_{h_a}}{\partial \delta_a}\right)_{C_{h_a}\,=\,0}$ with lift coefficient. Model in complete configuration; propellers removed.
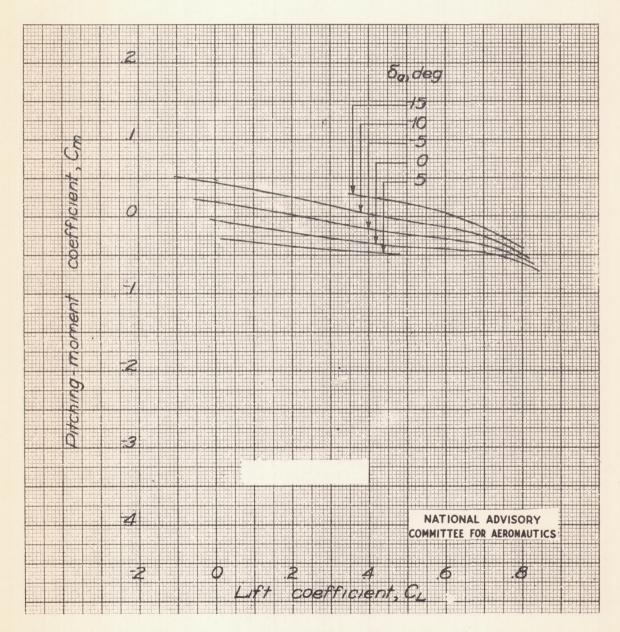
Figure 21.— Variation of pitching-moment coefficient with lift coefficient. Model in complete configuration; propellers removed.
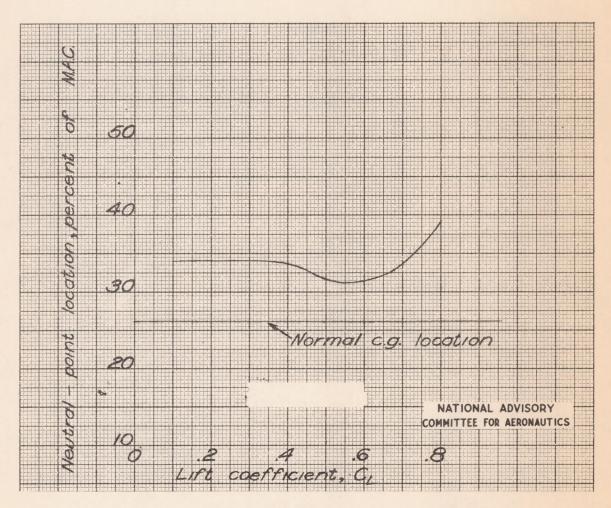
Figure 22.— Variation of stick—fixed neutral points with lift coefficient.
Model in complete configuration; propellers removed.
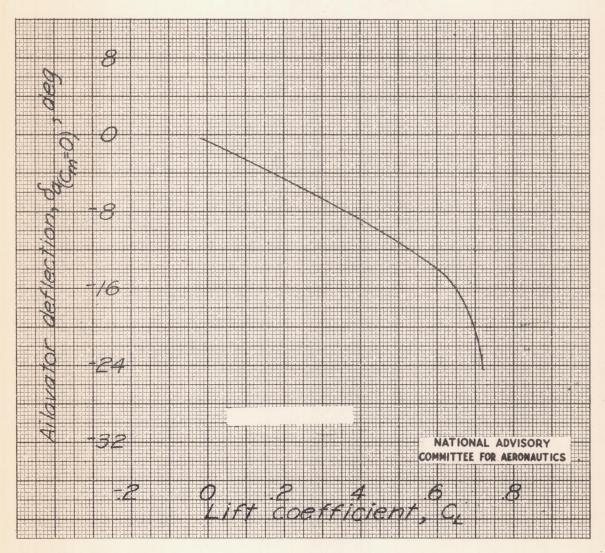
Figure 23.— Variation of ailavator deflection required for trim with lift
coefficient. Complete model configuration; propellers removed.
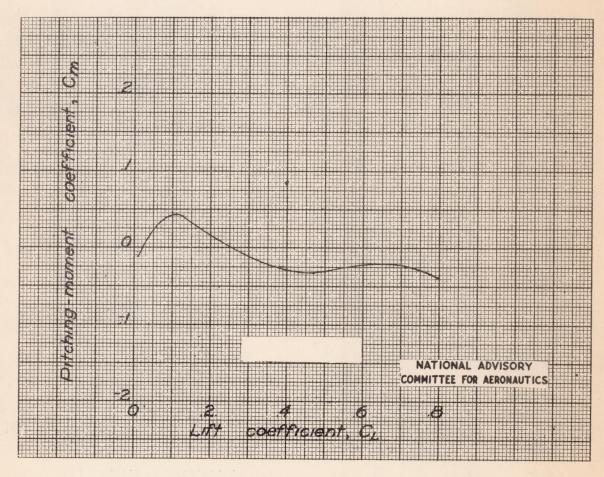
Figure 24.— Variation of pitching—moment coefficient with lift coefficient. $C_{h_a} = 0$. Model in complete configuration; propellers removed.
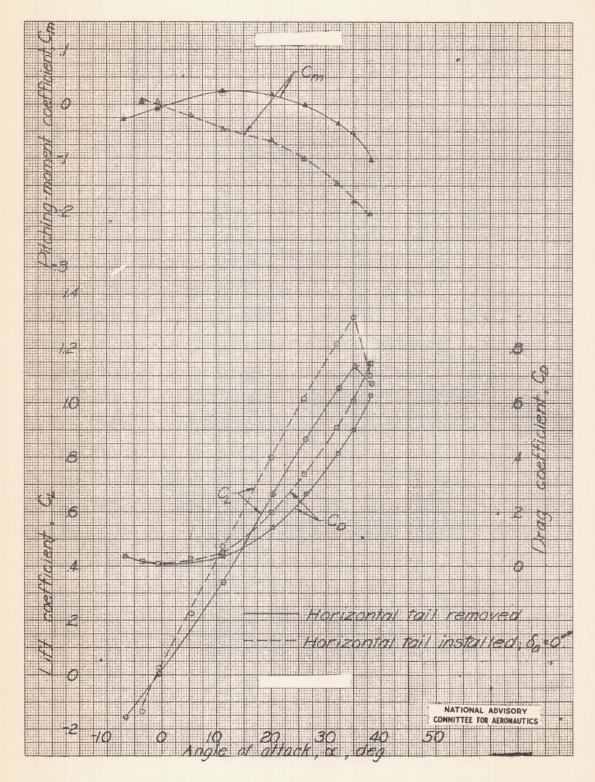
Figure 25.— Variation of C_L, C_D, and C_m with α of the model with the horizontal tail installed and removed. Basic model configuration; propellers removed.
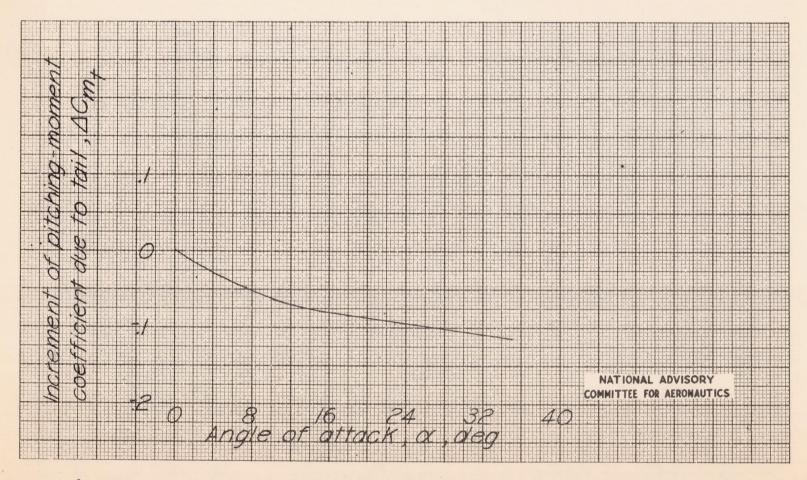
Figure 26.— Variation of increment of pitching—moment coefficient due to horizontal tail with angle of attack. Basic model configuration; propellers removed.
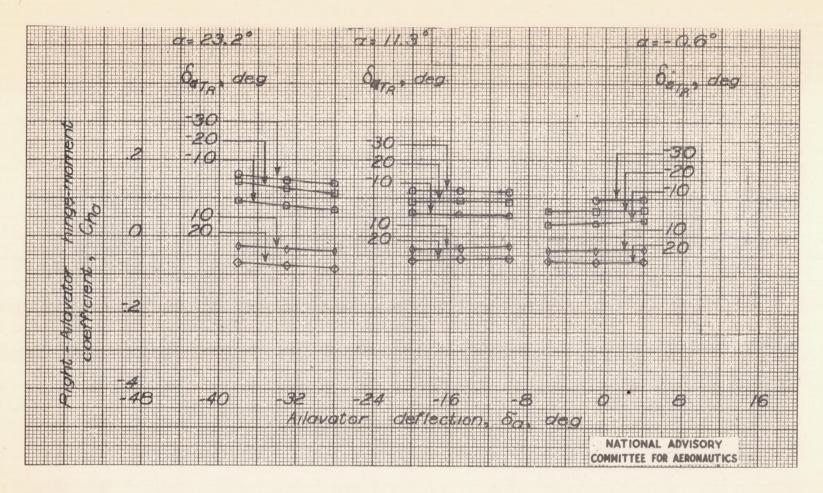
Figure 27.— The effect of right—ailavator tab setting on the variation of C_{h_a} with δ_a. Model in basic configuration; $\delta_{a_{TL}} = 0^\circ$; $\delta_r = 0^\circ$; propellers removed; $\delta_f = 0^\circ$.
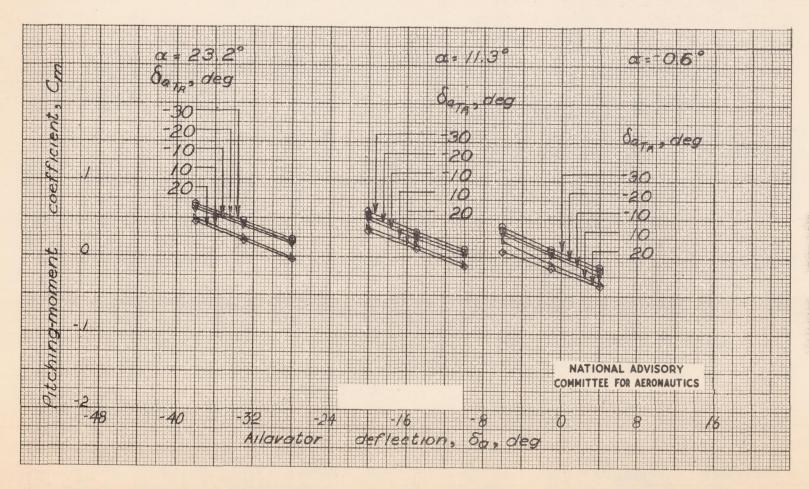
Figure 23.— The effect of right—ailavator tab setting on the variation of C_m with δ_a. Model in basic configuration; $\delta_{a_{T_L}} = 0^\circ$; $\delta_r = 0^\circ$; propellers removed; $\delta_f = 0^\circ$.
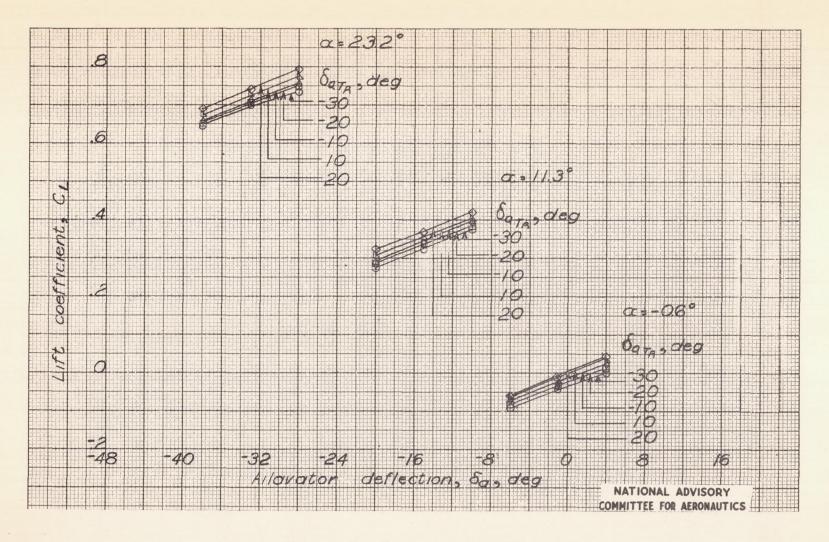
Figure 29.— The effect of right-ailavator tab setting on the variation of C_L with δ_a. Model in basic configuration; $\delta_{a_{T_L}} = 0^o$; $\delta_r = 0^o$; propellers removed; $\delta_f = 0^o$.
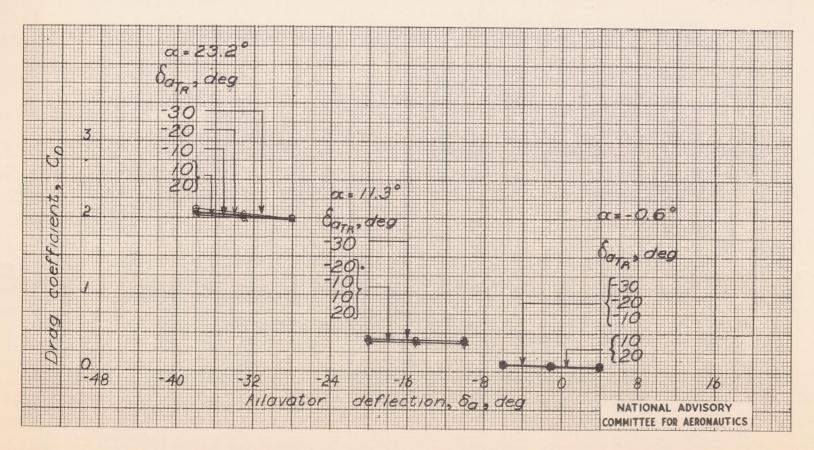
Figure 30.— The effect of right-ailavator tab setting on the variation of C_D with δ_a. Model in basic configuration; $\delta_{a_{T_L}} = 0°$; $\delta_r = 0°$; propellers removed; $\delta_f = 0°$.
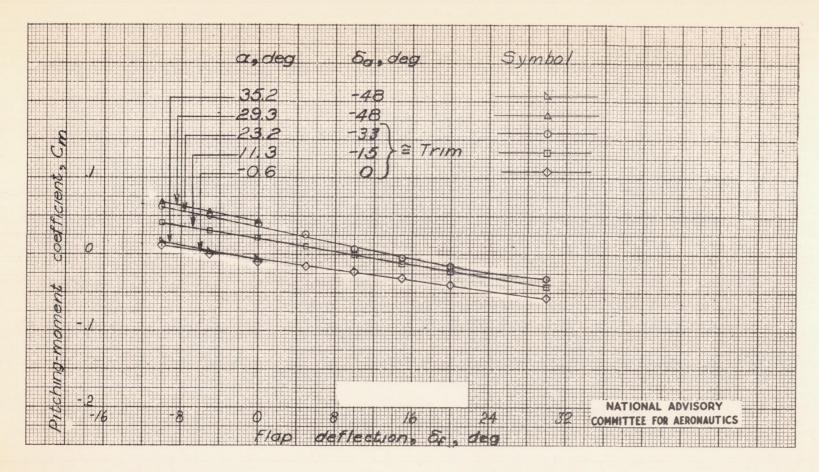
Figure 31.— Variation of pitching—moment coefficient with flap deflection. Model in basic configuration; $\delta_{a_{TL}} = \delta_{a_{TR}} = 0°$; $\delta_r = 0°$; propellers removed.
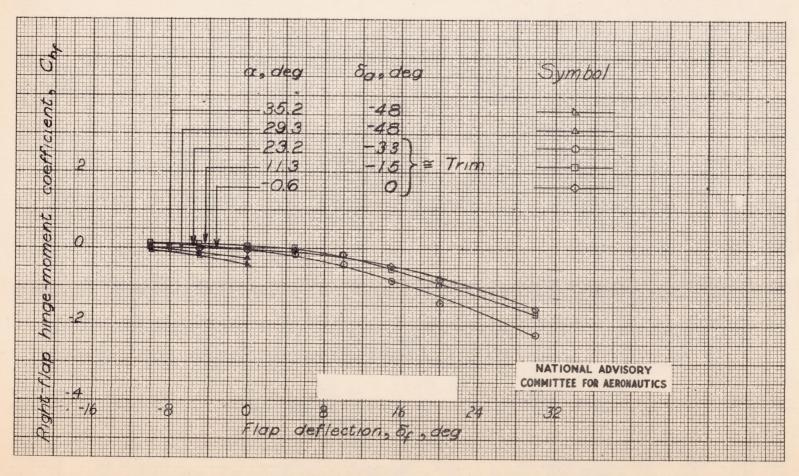
Figure 32.— Variation of right—flap hinge—moment coefficient with flap deflection.   Model in basic configuration; $\delta_{a_{T_L}} = \delta_{a_{T_R}} = 0°$; $\delta_r = 0°$; propellers removed.
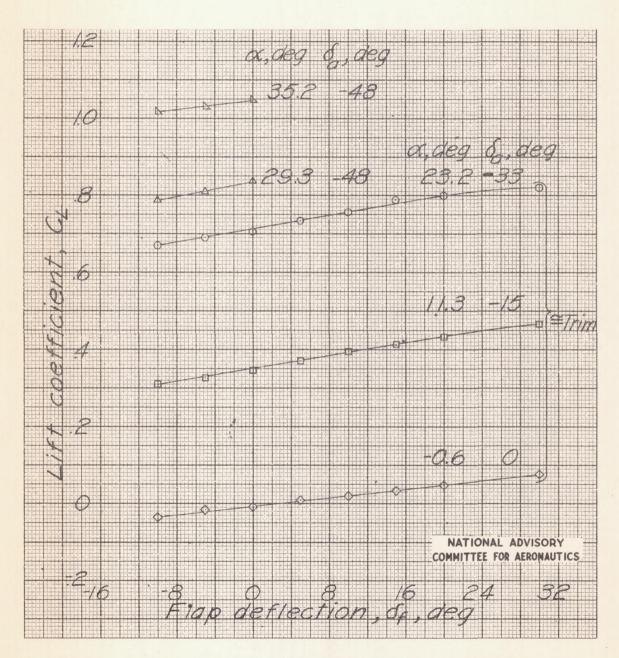
Figure 33.— Variation of lift coefficient with flap deflection. Basic
model configuration; $\delta_{a_{T_L}} = \delta_{a_{T_R}} = 0^o$; $\delta_r = 0^o$; propellers removed.
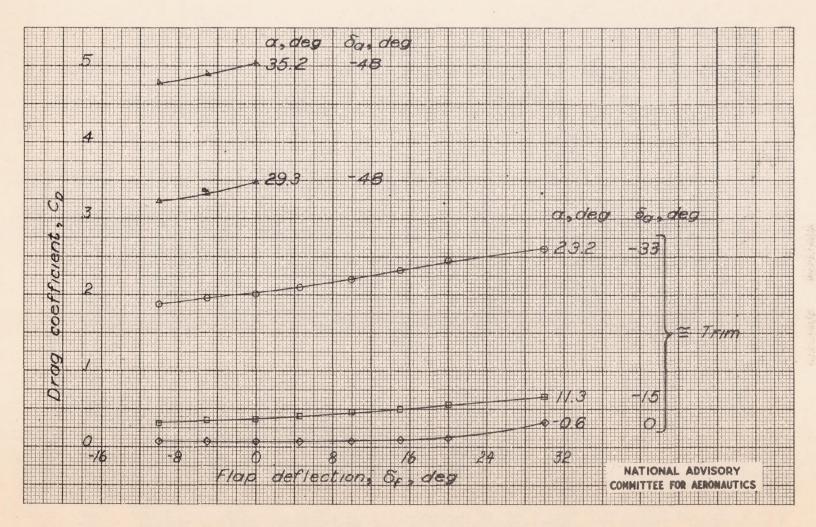
Figure 34.— Variation of drag coefficient with flap deflection. Model in basic configuration; $\delta_{a_{T_L}} = \delta_{a_{T_R}} = 0°$; $\delta_r = 0°$; propellers removed.
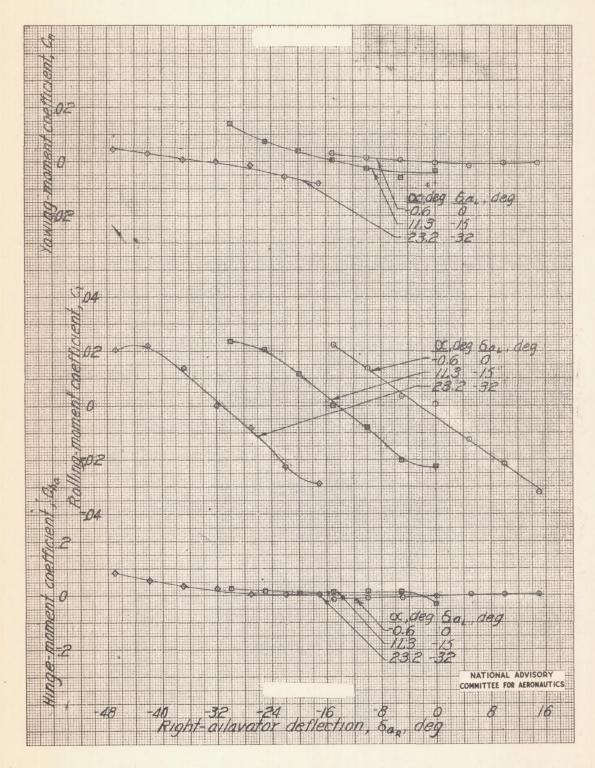
Figure 35.— Variation of C_{h_a}, C_l, and C_n with right-ailavator deflection on a $\frac{1}{3}$—scale model of the airplane. Left-ailavator fixed; propellers removed; V = 100 miles per hour; $\delta_r = 0°$; basic model configuration.
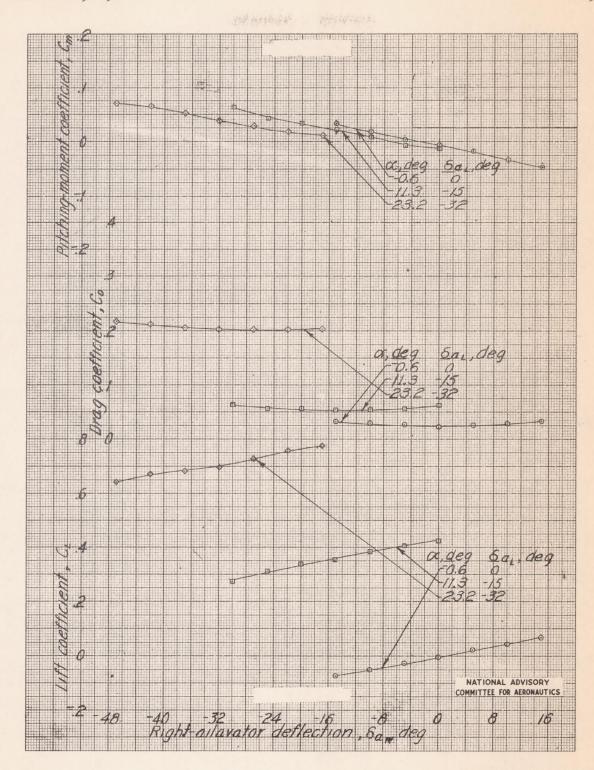
Figure 36.— Variation of C_L, C_D, and C_m with right-ailavator deflection on a $\frac{1}{3}$—scale model of the airplane. Left-ailavator fixed; propellers removed; V = 100 miles per hour; δ_r = 0°; basic model configuration.
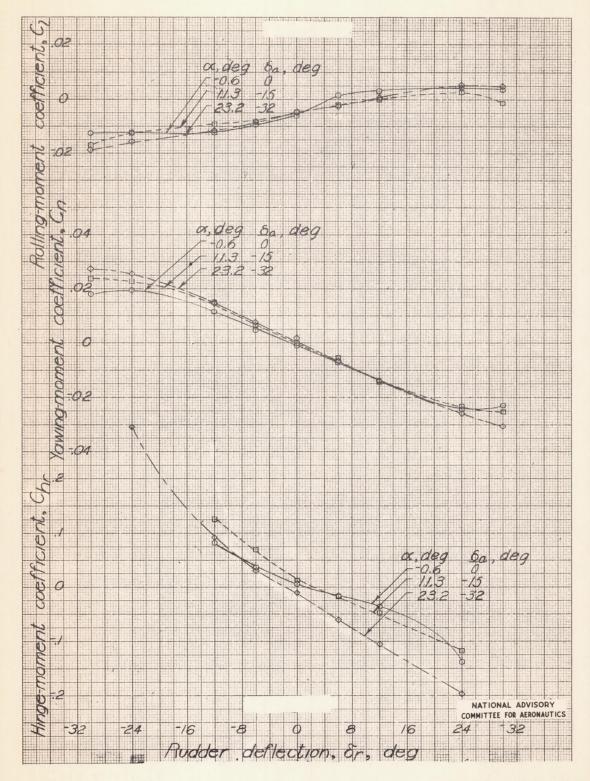
Figure 37.— Variation of C_{h_r}, C_n, and C_l with δ_r on a $\frac{1}{3}$—scale model of the airplane. Propellers removed; basic model configuration; V = 100 miles per hour.
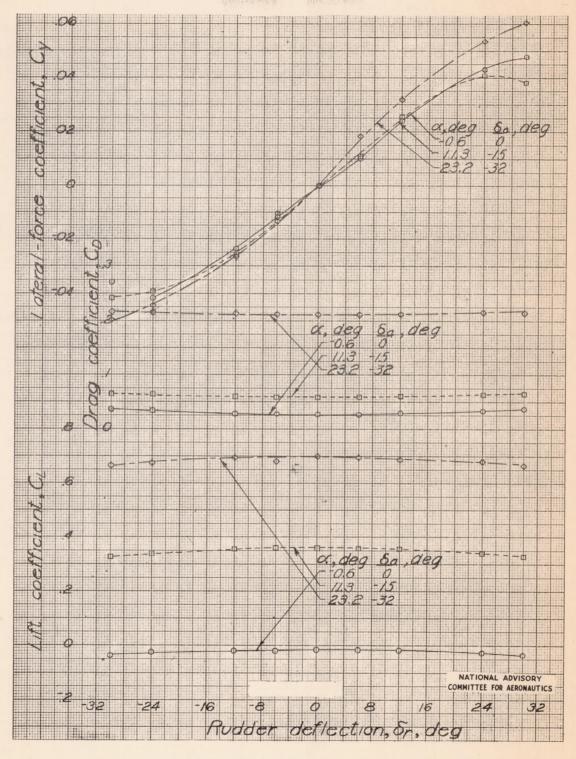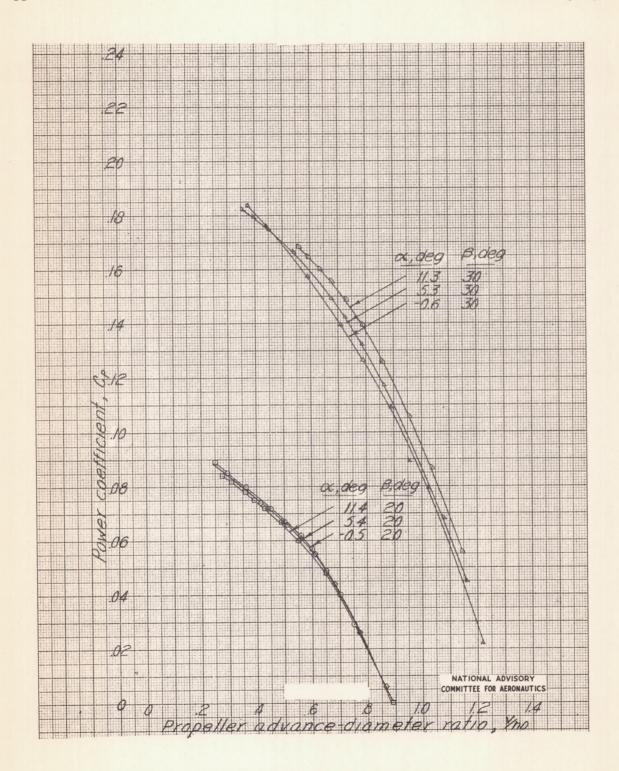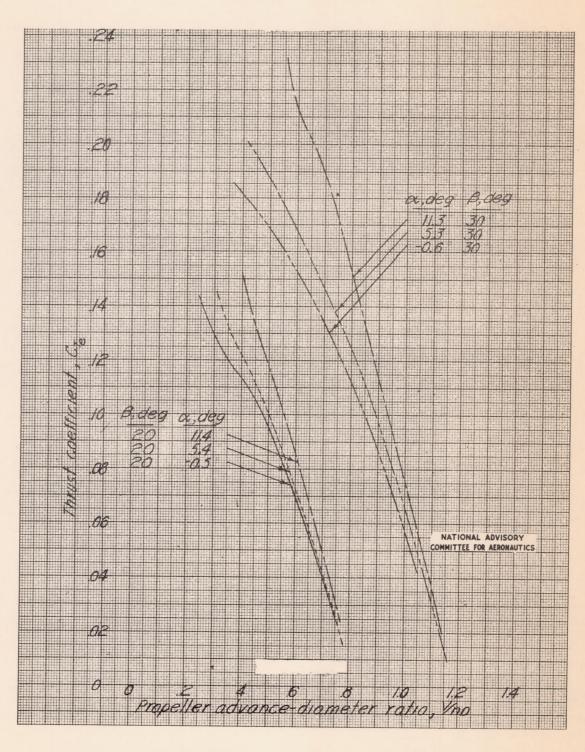
Figure 38.— Variation of C_L, C_D, and C_Y with δ_r on a $\frac{1}{3}$—scale model of the airplane. Propellers removed; basic model configuration; V = 100 miles per hour.
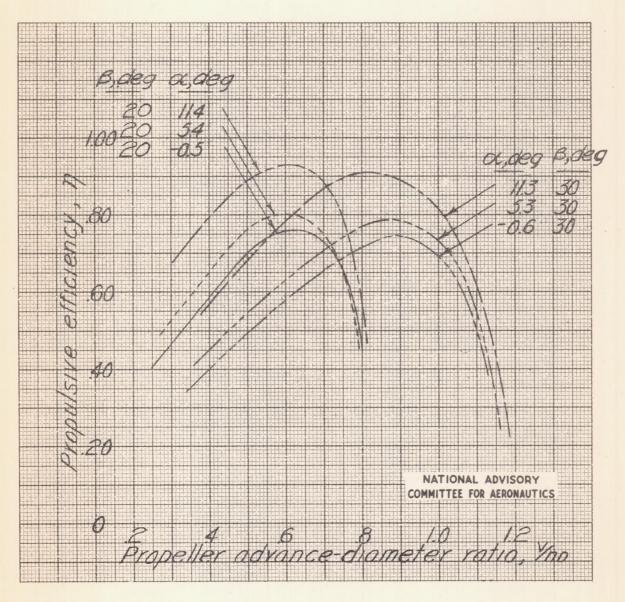
(a) Variation of C_p with V/nD.

Figure 39.— Typical curves showing propulsive characteristics. Basic
model configuration; all control surfaces neutral.

(b) Variation of C_{T_e} with V/nD.

Figure 39.— Continued.

(c) Variation of η with V/nD.

Figure 39.— Concluded.

(a) β = 20°.   (b) β = 30°.
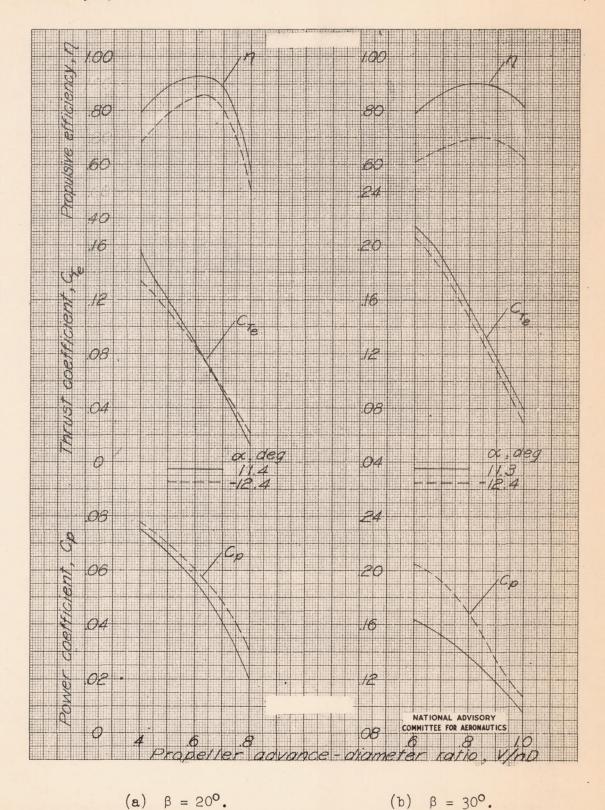
Figure 40.— Variation of C_p, C_{T_e}, and η with V/nD. Basic model
   configuration; all control surfaces neutral; data for β = 20°
   obtained with wing-tip support.
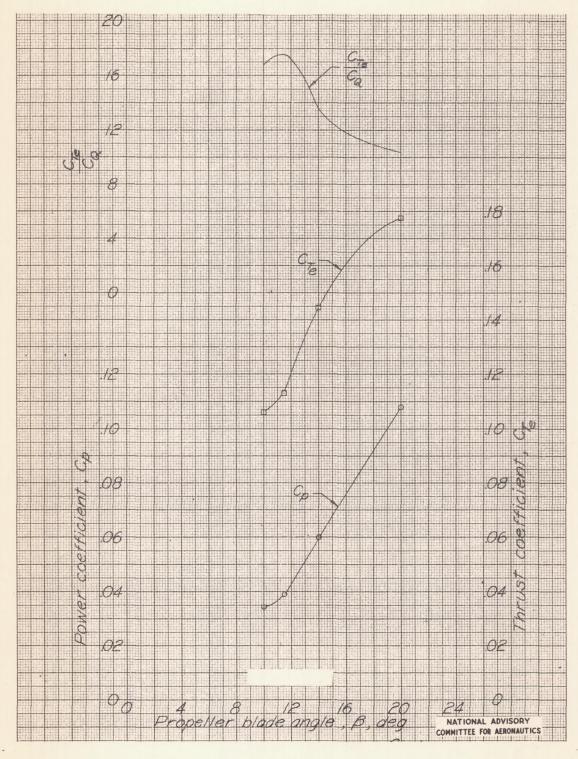
Figure 41.— Variation of C_p, C_{T_e}, and C_{T_e}/C_Q with β of the model propellers. Basic model configuration; $\frac{V}{nD} = 0$; data for $\beta = 20°$ obtained with wing–tip support.

(a) β = 20°.   (b) β = 30°.
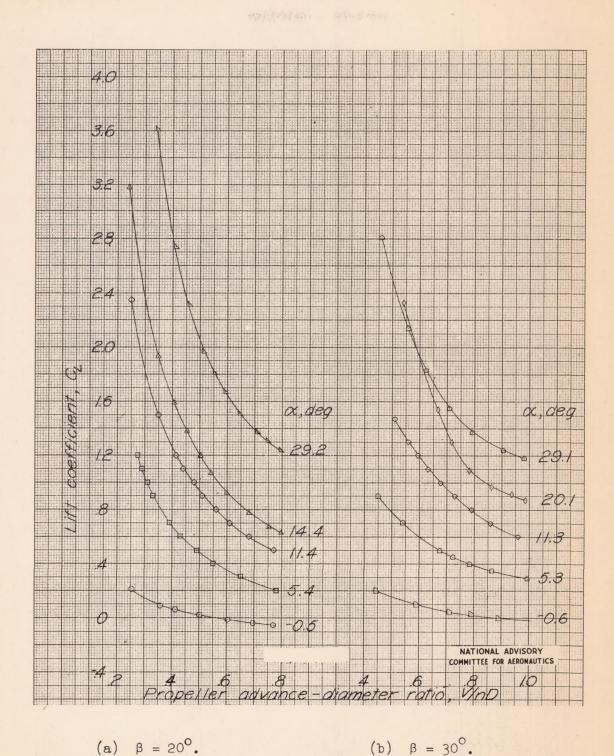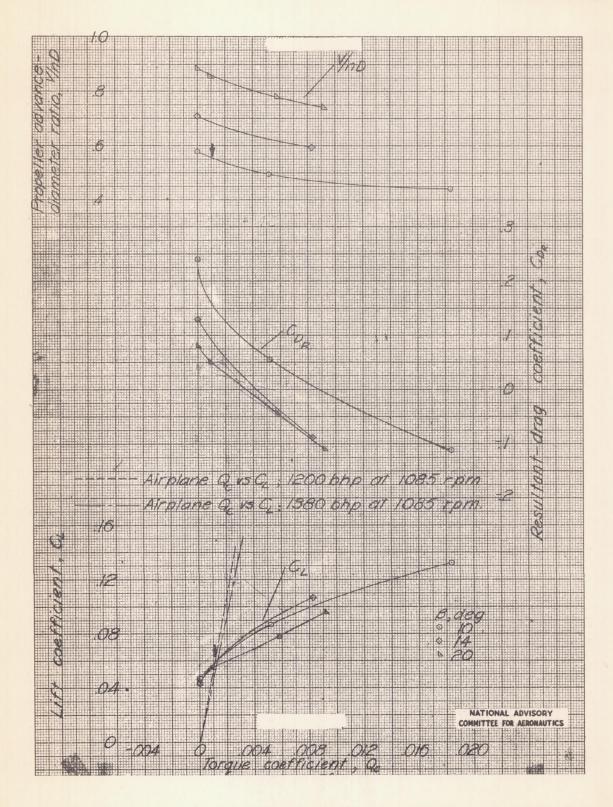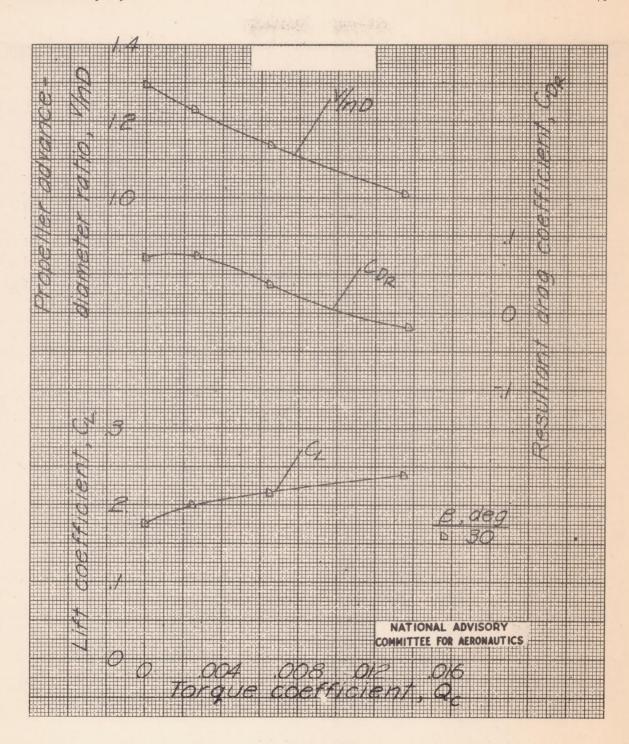
Figure 42.— Variation of C_L with V/nD. Basic model configuration; propellers operating; all control surfaces neutral; data β = 20° curves obtained with wing—tip support.
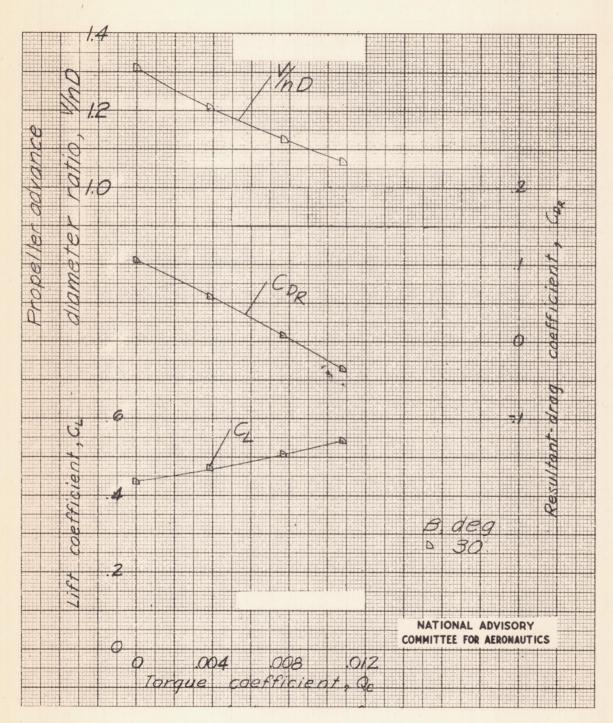
(a) $\alpha_u = 3^\circ$.

Figure 43.— Variation of C_L, C_{D_R}, and V/nD with Q_c for several
propeller blade angles. Basic model configuration; all control
surfaces neutral.
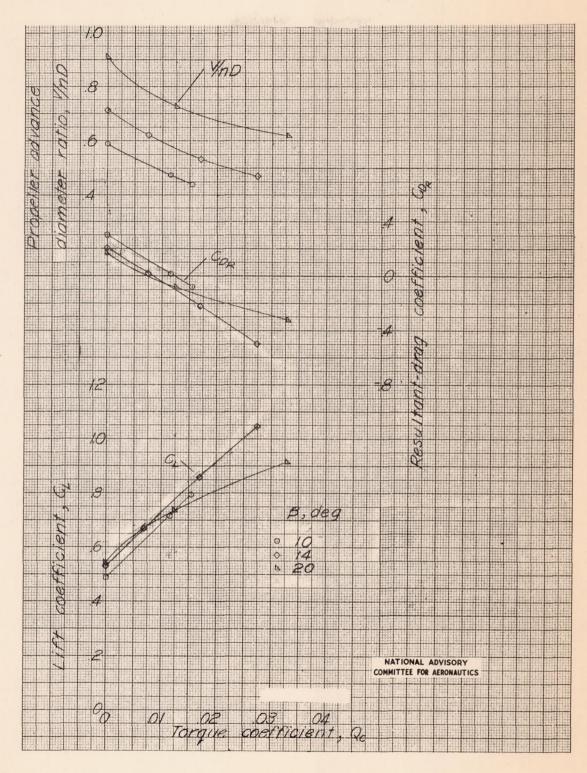
(b) $\alpha_u = 6°$.

Figure 43.- Continued.
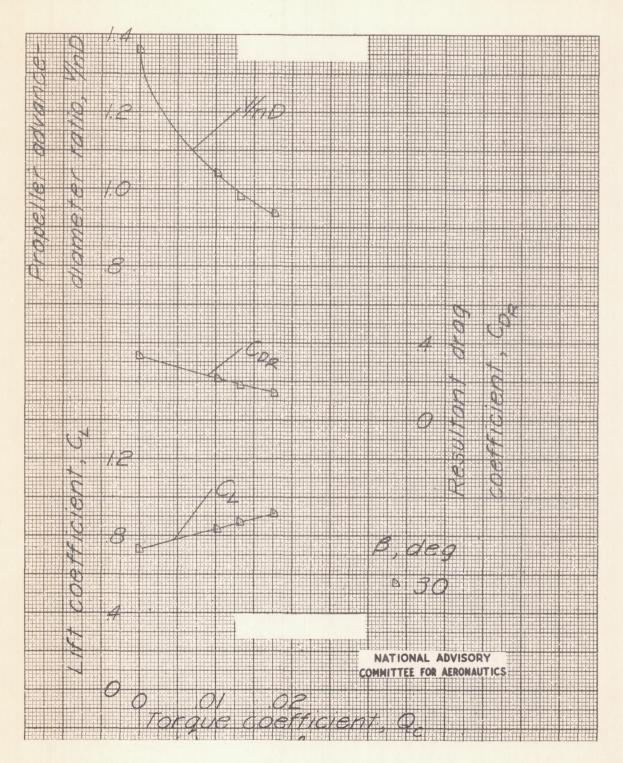
(c) $\alpha_u = 12^\circ$.

Figure 43.- Continued.
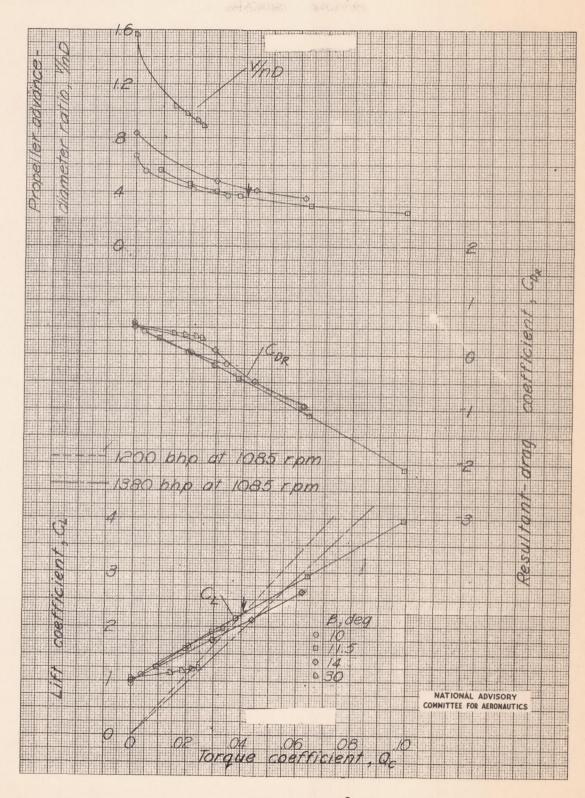
(d) $\alpha_u = 15°$.

Figure 43.— Continued.
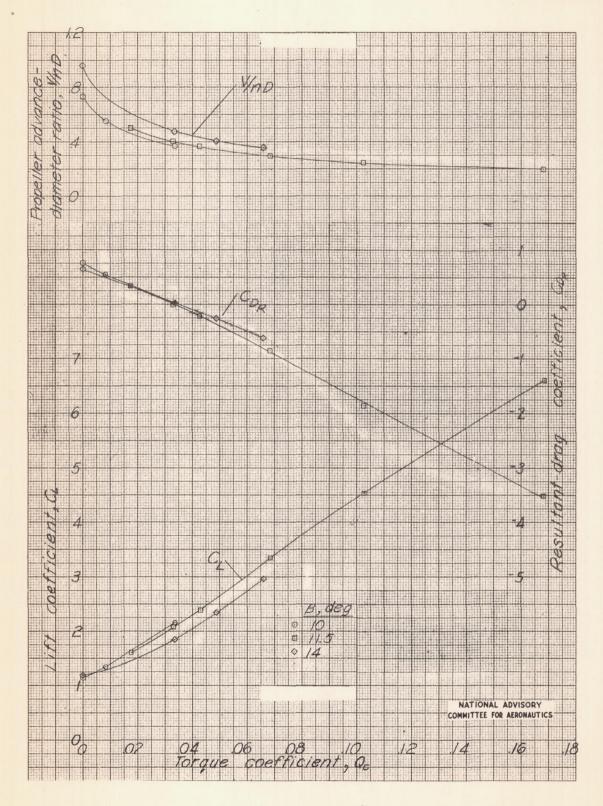
(e) $\alpha_u = 21°$.
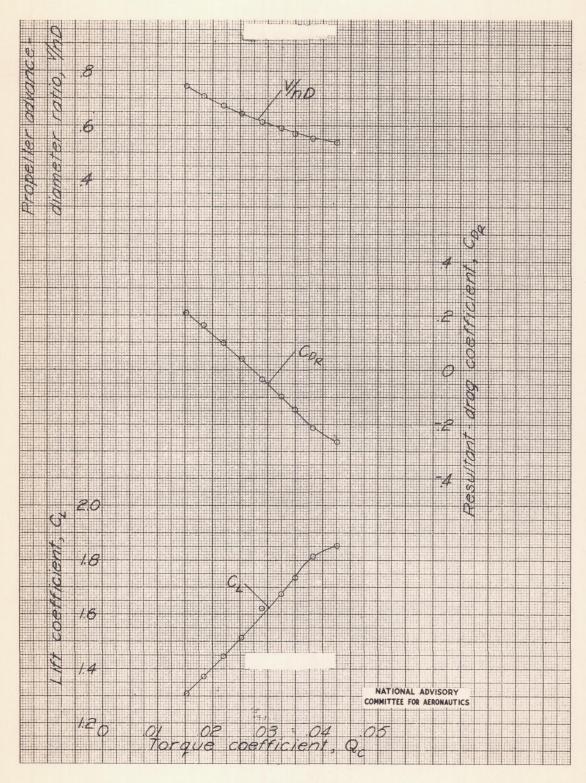
Figure 43.— Continued.

(f) $\alpha_u = 30°$.
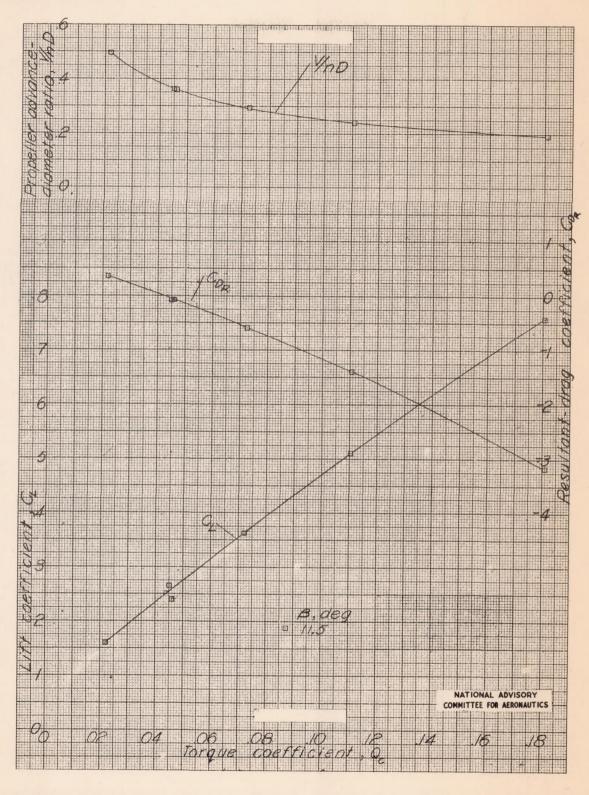
Figure 43.— Continued.
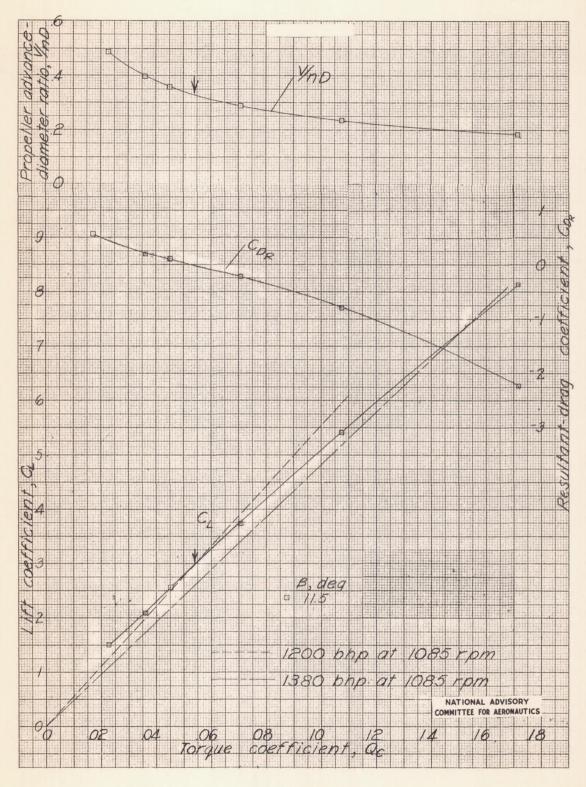
(g) $\alpha_u = 36^\circ$.

Figure 43.- Continued.
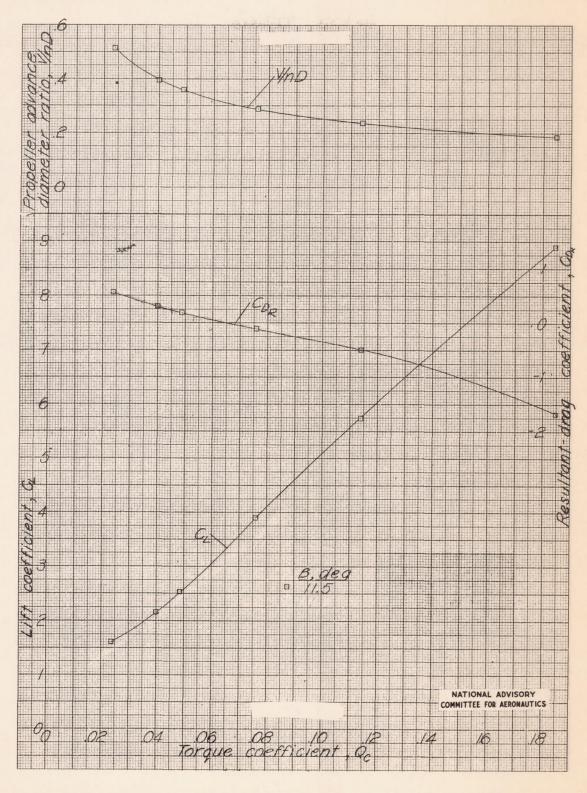
(h) $\alpha_u = 42°$.

Figure 43.— Continued.
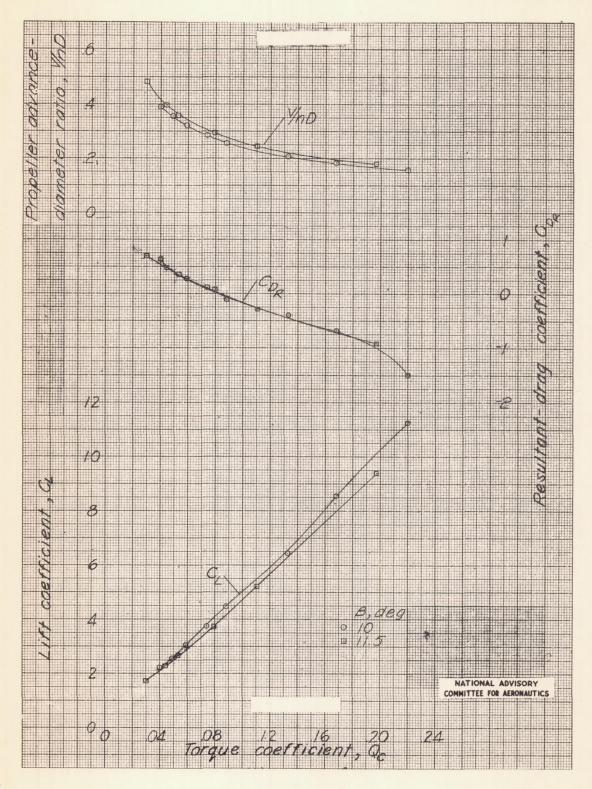
(i) $\alpha_u = 48^\circ$.

Figure 43.— Continued.
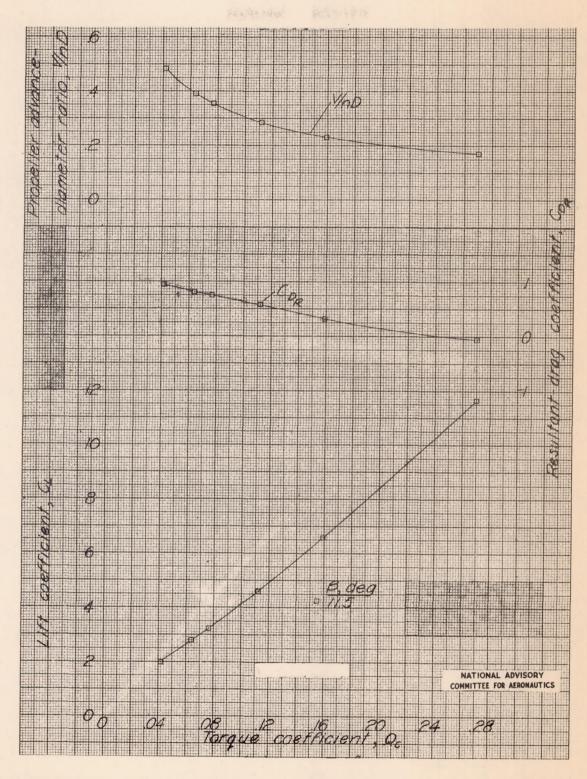
(j) $\alpha_u = 54°$.

Figure 43.- Continued.
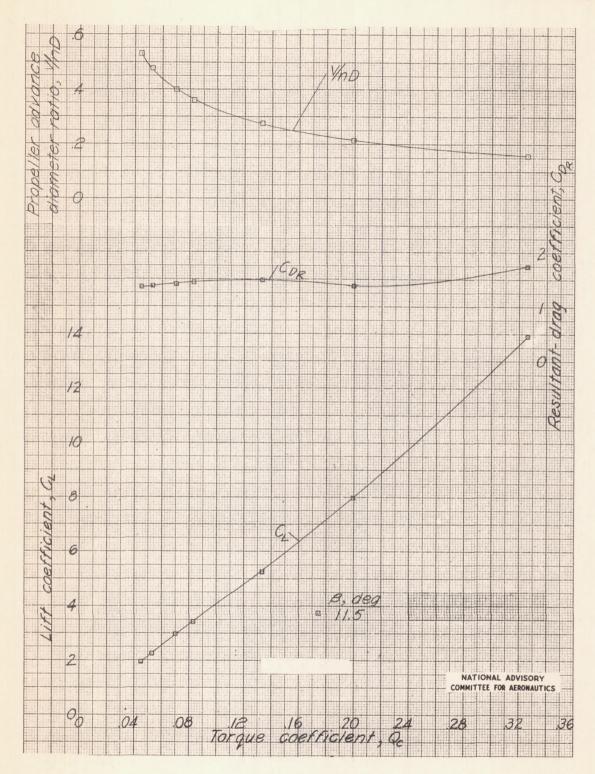
(k) $\alpha_u = 60°$.

Figure 43.— Continued.
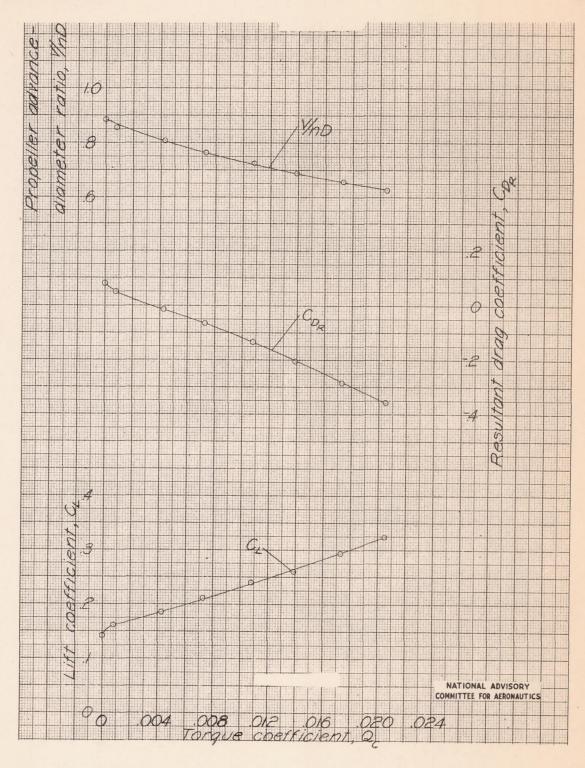
(l) $\alpha_u = 72°$.

Figure 43.— Continued.
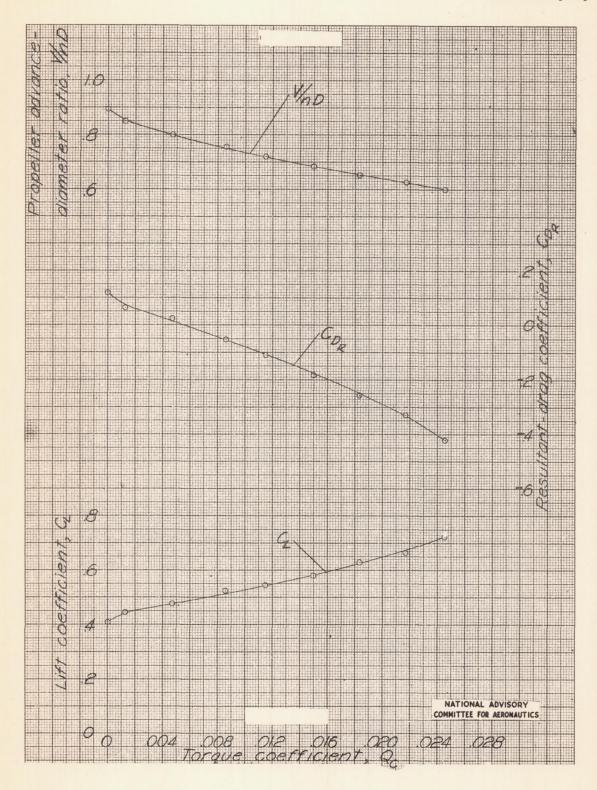
(m) $\alpha_u = 84°$.

Figure 43.— Concluded.
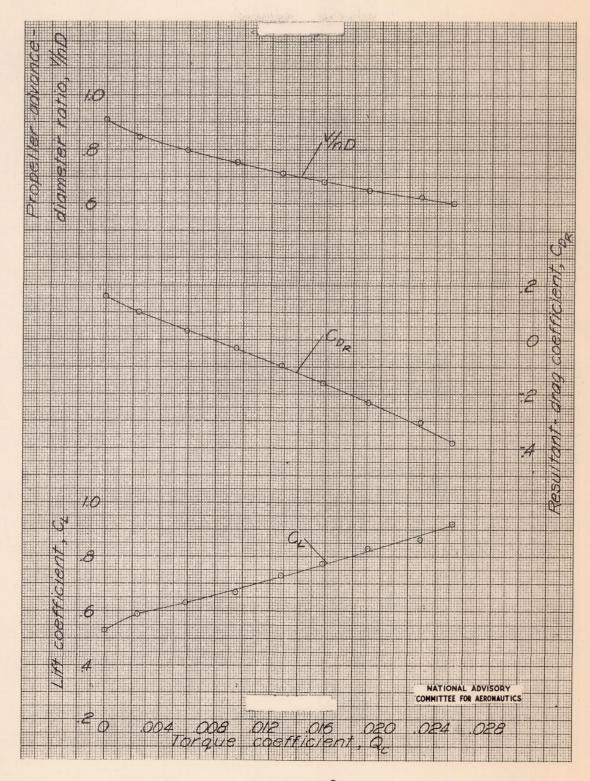
(a) $\alpha_u = 5°$.

Figure 44.— Variation of C_L, C_{D_R}, and V/nD with Q_c for $\beta = 20°$.

Basic model configuration; wing-tip support; all control surfaces neutral.

(b) $\alpha_u = 11^\circ$.

Figure 44.— Continued.
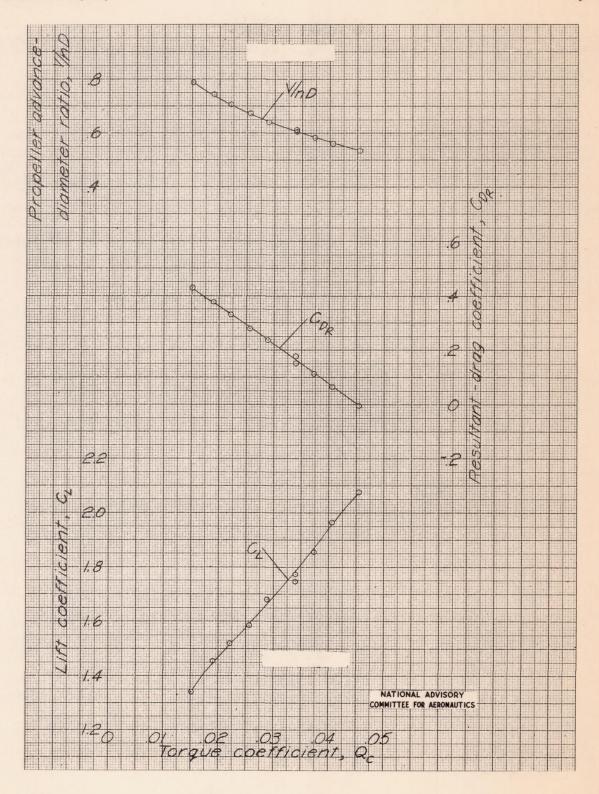
(c) $\alpha_u = 14°$.

Figure 44.— Continued.
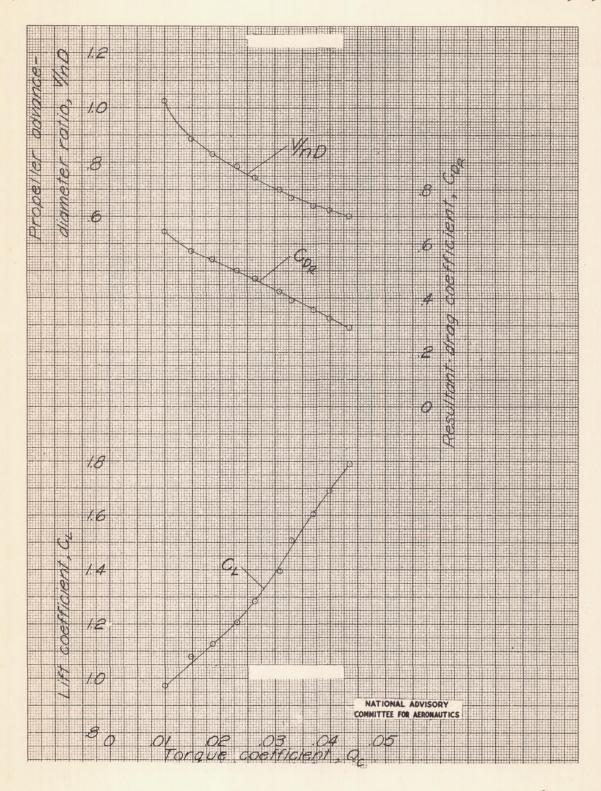
(d) $\alpha_u = 29°$.

Figure 44.— Continued.

(e) $\alpha_u = 35^o$.

Figure 44.— Continued.

(f) $\alpha_u = 44°$.

Figure 44.— Concluded.
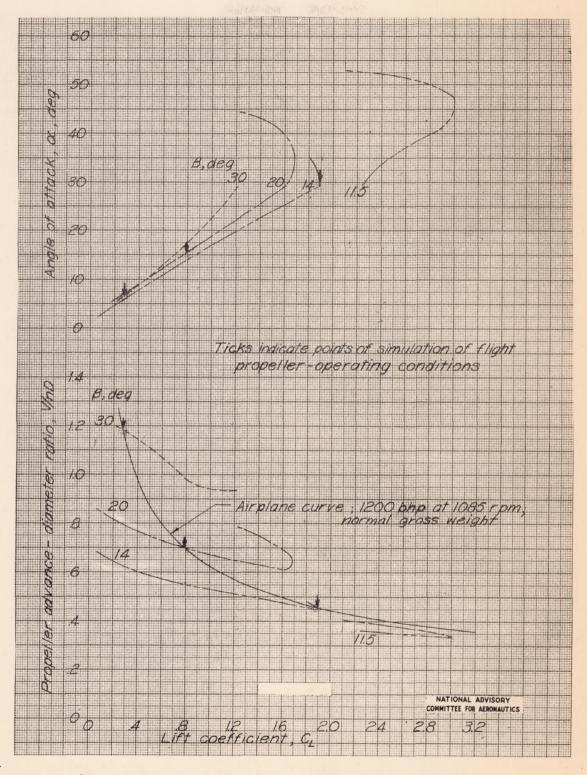
Figure 45.— Curves used for the determination of flight propeller-
operating lift coefficients from model data. Model curves
duplicate airplane Q_c against C_L for full-power operation;
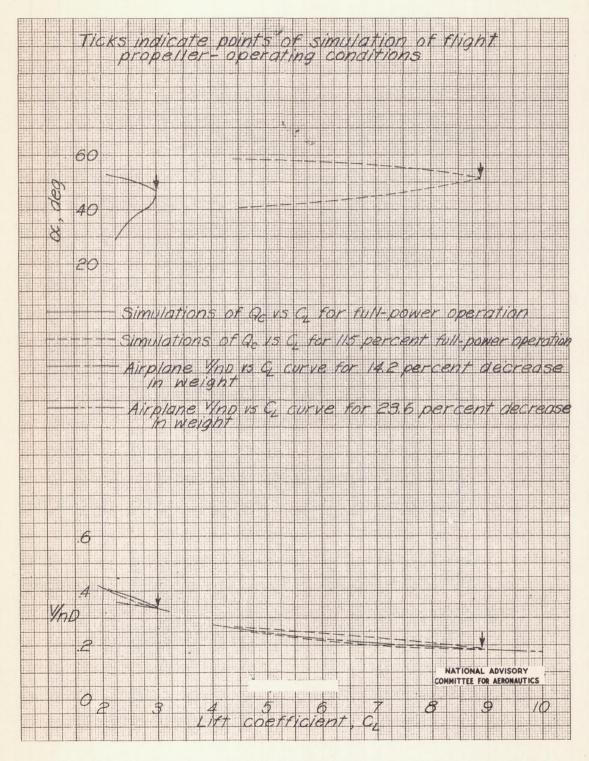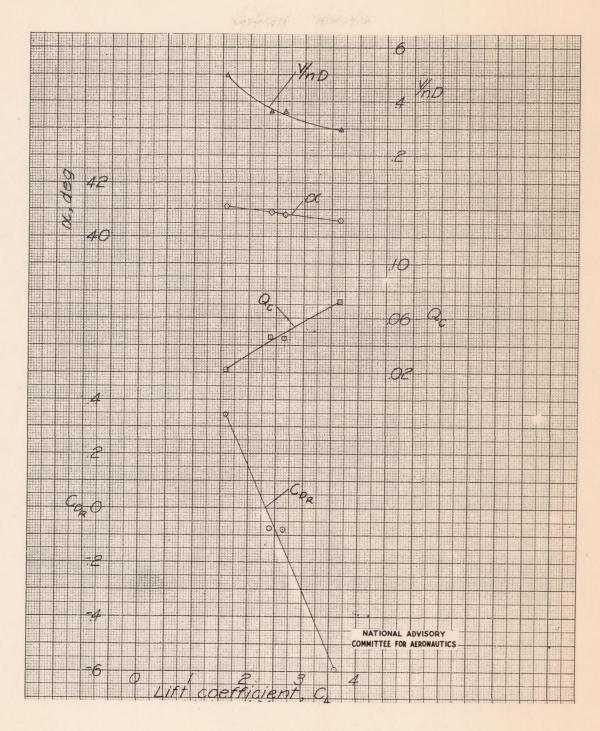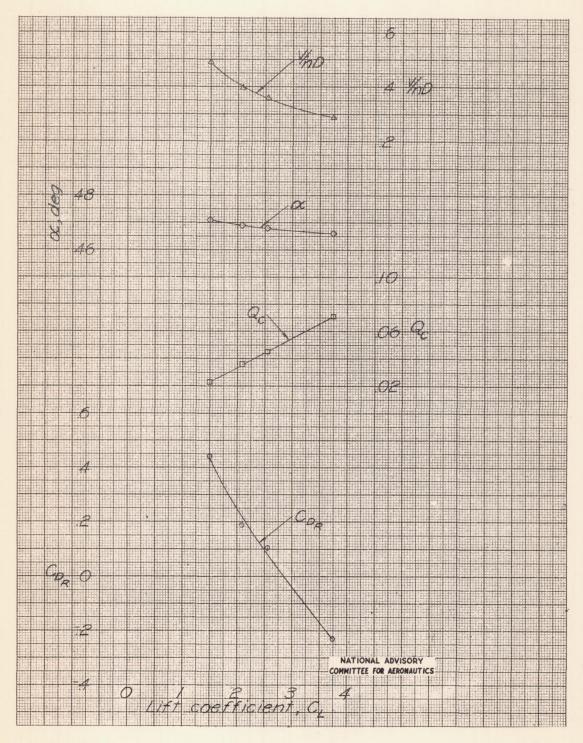basic model configuration; all controls neutral.

Ticks indicate points of simulation of flight
          propeller- operating conditions

α, deg

60

40

20

——————— Simulations of Q_c vs C_L for full-power operation

— — — — Simulations of Q_c vs C_L for 115 percent full-power operation

————————— Airplane V/nD vs C_L curve for 14.2 percent decrease
          in weight

————— — — Airplane V/nD vs C_L curve for 23.6 percent decrease
          in weight

.6

.4

V/nD

.2

0

NATIONAL ADVISORY
COMMITTEE FOR AERONAUTICS

2   3   4   5   6   7   8   9   10

Lift coefficient, C_L

Figure 46.— Curves used for the determination of flight propeller—
operating lift coefficients from model data at β = 11.5°. Basic
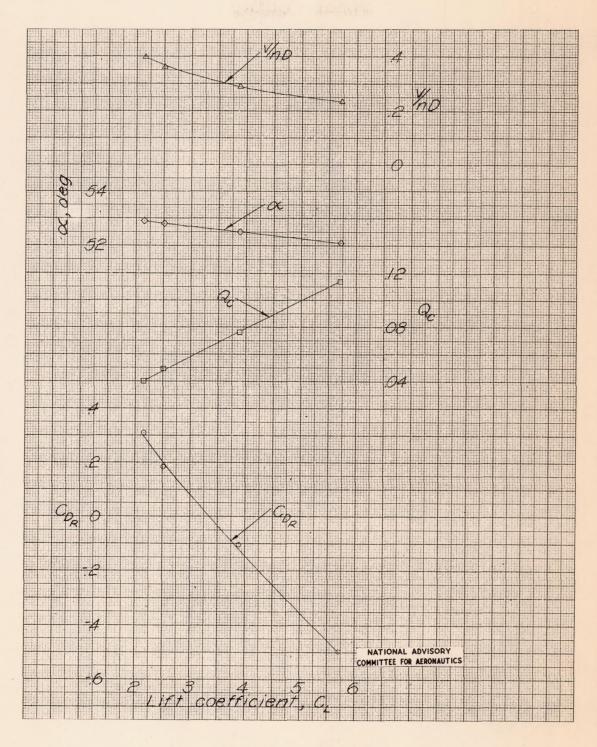model configuration; all controls neutral.

(a) $\alpha_u = 42^\circ$.

Figure 47.— Variation of C_{D_R}, Q_c, α, and V/nD with C_L for propeller
operation at $\beta = 11.5^\circ$. Basic model configuration; all control
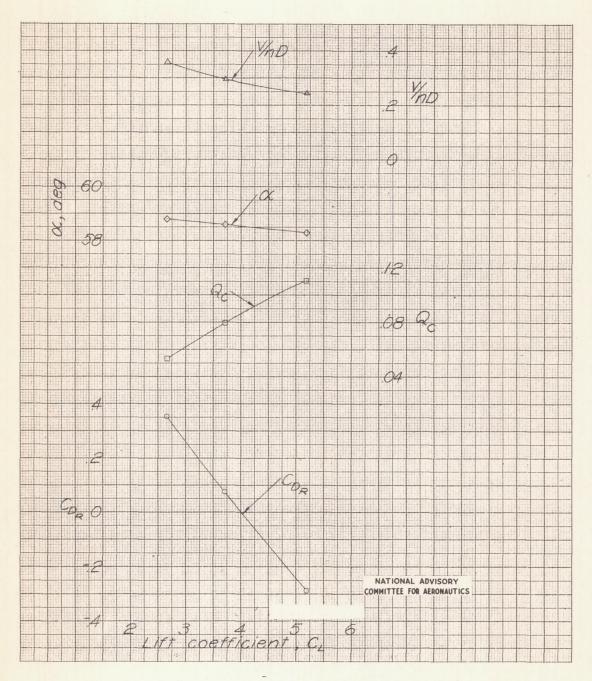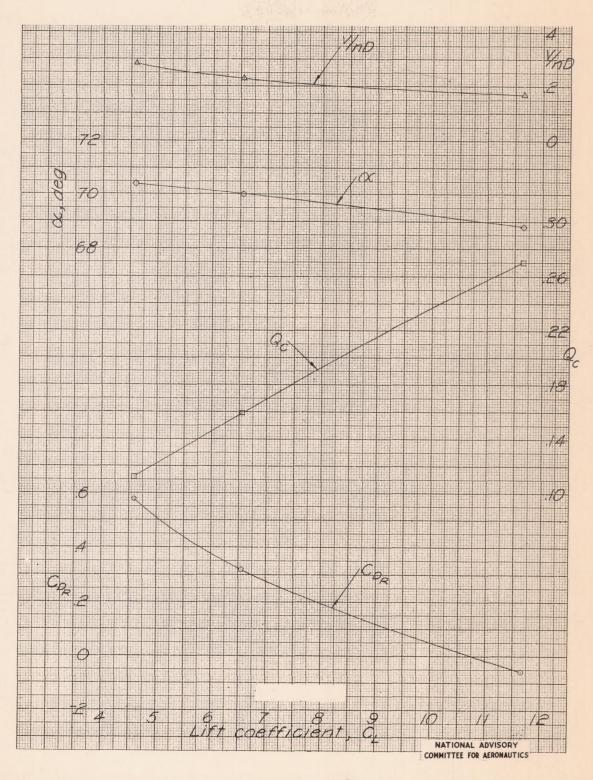surfaces neutral.

(b) $\alpha_u = 48°$.

Figure 47.- Continued.

(c) $\alpha_u = 54°$.

Figure 47.— Continued.

(d) $\alpha_u = 60^o$.

Figure 47.— Continued.

(e) $\alpha_u = 72^\circ$.

Figure 47.— Concluded.

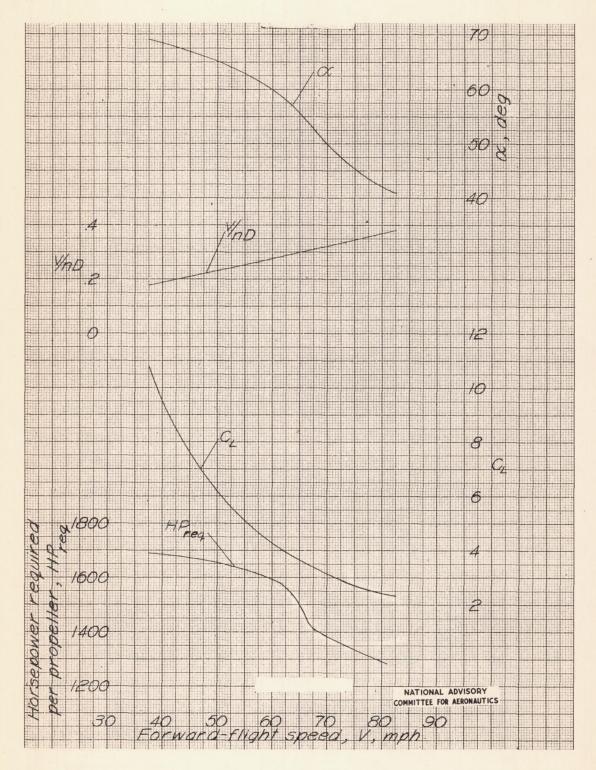Figure 48.— Variation of HP_{req}, C_L, V/nD, and α with V for level-
   flight conditions at $\beta = 11.5^\circ$. All control surfaces neutral;
   normal gross weight.